Marine and Petroleum Geology 132 (2021) 105224

Contents lists available at ScienceDirect

Marine and Petroleum Geology

journal homepage: www.elsevier.com/locate/marpetgeo

Improved method for quantitative evaluation of fault vertical sealing: A case study from the eastern Pinghu Slope Belt of the Xihu Depression, East China Sea Shelf Basin

Fuwei Wang [a,b], Dongxia Chen [a,b,*], Wenlei Du [a,b], Jianhui Zeng [a,b], Qiaochu Wang [a,b], Ziye Tian [a,b], Siyuan Chang [a,b], Mengya Jiang [a,b]

[a] State Key Laboratory of Petroleum Resources and Prospecting, China University of Petroleum (Beijing), Beijing, 102249, China
[b] College of Geosciences, China University of Petroleum (Beijing), Beijing, 102249, China

ARTICLE INFO

Keywords:
Fault vertical sealing
Quantitative evaluation
Hydrocarbon migration
Hydrocarbon accumulation
Xihu depression

ABSTRACT

Fault vertical sealing evaluation is significantly important for revealing hydrocarbon migration and accumulation processes and reducing exploration risks. Based on the analysis of the stress normal to the fault plane, the pore-fluid pressure and the compressive strength of fault rock, a new parameter, namely, the fault vertical sealing index (F_{VSI}), is proposed for improved quantitative evaluation. In this article, static faults distributed in the eastern Pinghu Slope Belt (EPSB) of the Xihu Depression are selected as examples. The vertical sealing properties of four major fault systems that control hydrocarbon distribution are analyzed and evaluated. The F_{VSI} value is positively correlated with the vertical sealing capacity of the fault zone, and the heterogeneous spatial distribution of the F_{VSI} along the fault planes indicates that a fault cannot be uniformly regarded as a conduit or a barrier. According to the relation between the F_{VSI} and the corresponding natural gas and oil shows, a fault zone with an F_{VSI} value less than 0.4 commonly acts as a vertical conduit and cannot accumulate hydrocarbons, while a fault zone with an F_{VSI} value greater than 0.4 has the ability to seal hydrocarbons. However, whether hydrocarbons can continue to migrate vertically depends on the maximum hydrocarbon column height that the corresponding F_{VSI} can seal. In this case study, fault zones with F_{VSI} values greater than 1 completely act as barriers to vertical hydrocarbon migration and no longer transport hydrocarbons. The changing F_{VSI} of the fault zone controls the process of hydrocarbon migration and accumulation, thereby affecting the distribution of hydrocarbons. In the structurally lower position of the EPSB with sufficient hydrocarbon sources, the weak vertically sealed fault zone commonly causes a vertical multilayered distribution of hydrocarbons. Conversely, in the structurally higher position of the EPSB with insufficient hydrocarbon charging, the strong vertically sealed fault zone results in a more concentrated hydrocarbon distribution in the lower strata. However, there are no natural gas and oil shows in the fault zone that completely act as vertical conduits. Therefore, the F_{VSI} can be an effective quantitative method to analyze vertical hydrocarbon migration pathways and accumulation locations controlled by faults and has great application potential in reducing the risks in petroleum exploration projects.

1. Introduction

Faults are important geologic structures because they can act as either conduits or barriers for subsurface hydrocarbon migration (Gibson, 1994; Knipe, 1997; Karlsen and Skeie, 2006; Zhang et al., 2010). Natural examples have confirmed that a fault is not a simple single-plane but a zone consisting of a fault core and a surrounding damage zone (Knipe et al., 1997; Schultz and Fossen, 2008; Faulkner et al., 2010). Generally, the fault core accommodates most of the displacement and generates different fault rocks when different types of host rocks are entrained into the fault zones, while the damage zone may be composed of subsidiary faults and fractures over a wide range of length scales (Faulkner et al., 2003, 2010; Pei et al., 2015). For this reason, the migration of hydrocarbon within the fault zone is complicated, and the major mechanisms can be summarized as the capillary/permeability leakage in the static period and fault movement (or

* Corresponding author. State Key Laboratory of Petroleum Resources and Prospecting, China University of Petroleum (Beijing), Beijing, 102249, China.
E-mail address: lindachen@cup.edu.cn (D. Chen).

https://doi.org/10.1016/j.marpetgeo.2021.105224
Received 22 December 2020; Received in revised form 16 June 2021; Accepted 7 July 2021
Available online 9 July 2021

reactivation) induced by tectonic motion or overpressure (or a combination of both) (Schowalter, 1979; Gartrell et al., 2006; Manzocchi and Childs, 2013; Hao et al., 2015). As the fault movement is usually episodic, highly complex fault zones may provide different preferential conduits for fluid flow in different fault evolution stages (Caine et al., 1996; Bense et al., 2013; Indrevær et al., 2014). During the faulting processes, fluids driven by the "seismic pumping" preferentially flow through the opened fractures in the fault core and damage zone with a relatively high velocity (Sibson et al., 1975; Hao et al., 2009; Indrevær et al., 2014; Blouet et al., 2017), and may result in complete loss of accumulated petroleum (Gartrell et al., 2006; Zhang et al., 2009a, b). However, during a longer period of fault quiescence, fluids driven by buoyancy mainly flow through the connected pore system in the fault rock instead of the closed fractures (Fu et al., 2008; Indrevær et al., 2014). For this stage, the migration and accumulation of hydrocarbon related to faults predominantly depends on the capillary/permeability sealing of the fault rock (Fisher and Knipe, 2001; Fisher and Jolley, 2007), which can be assessed by different qualitative and quantitative methods.

Fault-sealing capability can be defined as the maximum hydrocarbon column height that the fault seal is capable of supporting before hydrocarbons start to leak through the seal. In this way, the fault zone can be served as a conduit for the hydrocarbon migration when the hydrocarbon column height breaks through the fault seal. Otherwise, the static fault zone acts as a permeability barrier. Previous research has studied the sealing behavior of fault zones (Fisher and Knipe, 1998; Fossen et al., 2007; Fisher et al., 2009) and proposed many fundamental controlling factors and evaluation methods. On the whole, fault-sealing capability can be evaluated by the lateral sealing capability and the vertical sealing capability because faults have two directions for fluid migration. For lateral sealing, evaluation methods such as stratigraphic juxtaposition (Allan, 1989; Knipe, 1997), clay smear indices (Bouvier et al., 1989; Lindsay et al., 1993; Fulljames et al., 1997; Yielding et al., 1997), and displacement pressure differences (Lü et al., 2009; Fu et al., 2012; Lei et al., 2013) have been widely used to effectively evaluate the ability of faults to seal hydrocarbon laterally. Moreover, the effect of buoyancy determines that hydrocarbons preferentially leak upwards when the hydrocarbon column height exceeds the vertical capillary/permeability seal. Researchers have evaluated different aspects of fault vertical sealing. According to the stress field, the component of the effective stress normal to the fault plane is an essential factor that causes fracture closure and plastic rock deformation (Harding and Tuminas, 1989; Ho et al., 2016, 2018). The quantitative method of normal stress proposed by Jaeger and Cook (1979), Lü et al. (1996) and Fu et al. (1998) has been widely used to determine fault vertical sealing. In these methods, the fault zone is regarded as the surface or homogeneous unit to determine the tightness, while ignoring its internal heterogeneity. On the other hand, considering the components of fault rocks, the ratio of normal stress to compressive strength of the fault rock has been proposed to characterize vertical sealing properties (Tian et al., 2003; Li et al., 2020). However, this method fails to include the variation of rock compressive strength with burial depth (Peng, 1993; Tang et al., 2016). Additionally, a high pore-fluid pressure tends to cause fault zones to reactivation or hydrofracturing and behave as vertical conduits for hydrocarbon migration (Sibson et al., 1975; Sibson, 1990; Byerlee, 1993; Luo, 2004; Ho et al., 2012). For this reason, the relative magnitude between pore-fluid pressure and stress normal to the fault plane has also been defined to characterize the vertical sealing capability (Tong, 1998).

Nevertheless, current methods for evaluating the fault vertical sealing properties are mainly focused on certain aspects instead of serving as comprehensive analyses involving multiple control factors, which restricts the migration analysis related to vertical fault sealing. Further systematic analysis and quantitative research are still required to increase the accuracy of sealing evaluation and to reduce the hydrocarbon exploration risk in the rift basins. The static faults distributed in the eastern Pinghu Slope Belt (EPSB) of the Xihu Depression of the East China Sea Shelf Basin can provide a case study for further investigation. The EPSB is characterized by the development of normal fault systems with active duration earlier than the hydrocarbon charging period (Zhang, 2013; Shan et al., 2015). Although there is no rapid fluid flow caused by "seismic pumping", the hydrocarbons have overcome the vertical seal of static faults and migrated into shallow reservoirs during the hydrocarbon charging period (Shan et al., 2015; Su et al., 2020). Therefore, the investigation of fault vertical sealing is necessary to understand the reasons for differential hydrocarbon distribution and migration process. In this article, based on the systematic analysis of the stress normal to the fault plane, the pore-fluid pressure, the compressive strength of fault rock and their influence on the hydrocarbon sealing behavior of the fault zone, an improved quantitative evaluation method, the fault vertical sealing index (F_{VSI}), is proposed to clarify the vertical sealing properties of faults. Moreover, the relations between the F_{VSI} and hydrocarbon migration, accumulation and distribution are systematically revealed. An evaluation method that combines multiple factors is important to accurately determine the fault sealing capacity. Furthermore, detailed insight into the relation between fault vertical sealing properties and vertical hydrocarbon migration and accumulation can provide further guidance for drilling and minimize exploration risks.

2. Geological setting

The East China Sea Shelf Basin is a back-arc rift basin in offshore China with the central Xihu Depression being an exploration focus (Duan et al., 2017; Zhang et al., 2018) (Fig. 1a). The Xihu Depression, occupying a surface area of approximately 46,000 km^2, is bounded by the Hupijiao, Haijiao, and Yushan Uplifts in the west and the Diaoyu Islands Uplift in the east. In detail, it can be further subdivided into four subunits, from west to east, namely the West Slope Belt, the Western Sub Sag (WSS), the Central Anticline Belt, and the Eastern Fault-fold Belt (Fig. 1b).

Tectonically, the Xihu Depression evolved through sequences of a rifting stage (65–32.0 Ma), a thermal depression stage (32.0–5.0 Ma) and a regional subsidence stage (5.0 Ma-present) (Ye et al., 2007; Zhang et al., 2009a, b). During the rifting stage, the upwelling of deep-hot mantle material and the underlying asthenosphere have caused intense rifting, leading to the formation of a series of grabens and half grabens along the major north-northeast trending fault set. Under the NW-SE-oriented extensional stress, major tectonic movements including Yandang Movement, Qujiang Movement and Yuquan Movement occurred in this stage, which resulted in the development of normal fault systems and the deposition of a thick sedimentary sequence (Song et al., 2010; Abbas et al., 2018). At time of thermal depression, the Huagang Movement and the Longjing Movement occurred due to the NW-SE-oriented compressive stress, and the sediments were slowly buried as the weakening of fault activity. Subsequently, under the control of NE-SW-oriented compressive stress, the Xihu Depression entered a period of regional subsidence in Pliocene and continued until Quaternary.

Sediments of the Paleogene-Neogene strata in the Xihu Depression include the fluvial-delta-lacustrine, fjord-tidal flat, and shallow marine deposits (Abbas et al., 2018). During the rifting stage, the sediments were restricted to grabens and half-grabens and were mainly composed of the Baoshi Formation (E_2b) deposited in a delta-estuarine environments and the Pinghu Formation (E_2p) dominated by fjord-tidal flat deposit. The Pinghu Formation (E_2p) is characterized by interbedded sandstone and mudstone, which can be further subdivided into three members, E_2p_3, E_2p_2, and E_2p_1, from bottom to top. The thermal depression stage filled the Huagang, Longjing, Yuquan and Liulang Formations deposited in fluvial-delta-lacustrine environment, and is overlain by thick mudstones of the Santan and Donghai Formations deposited during the subsidence stage.

For petroleum systems, the E_2p_3 Formation dominated by coals and carbonaceous dark mudstones serves as the primary source rocks in the

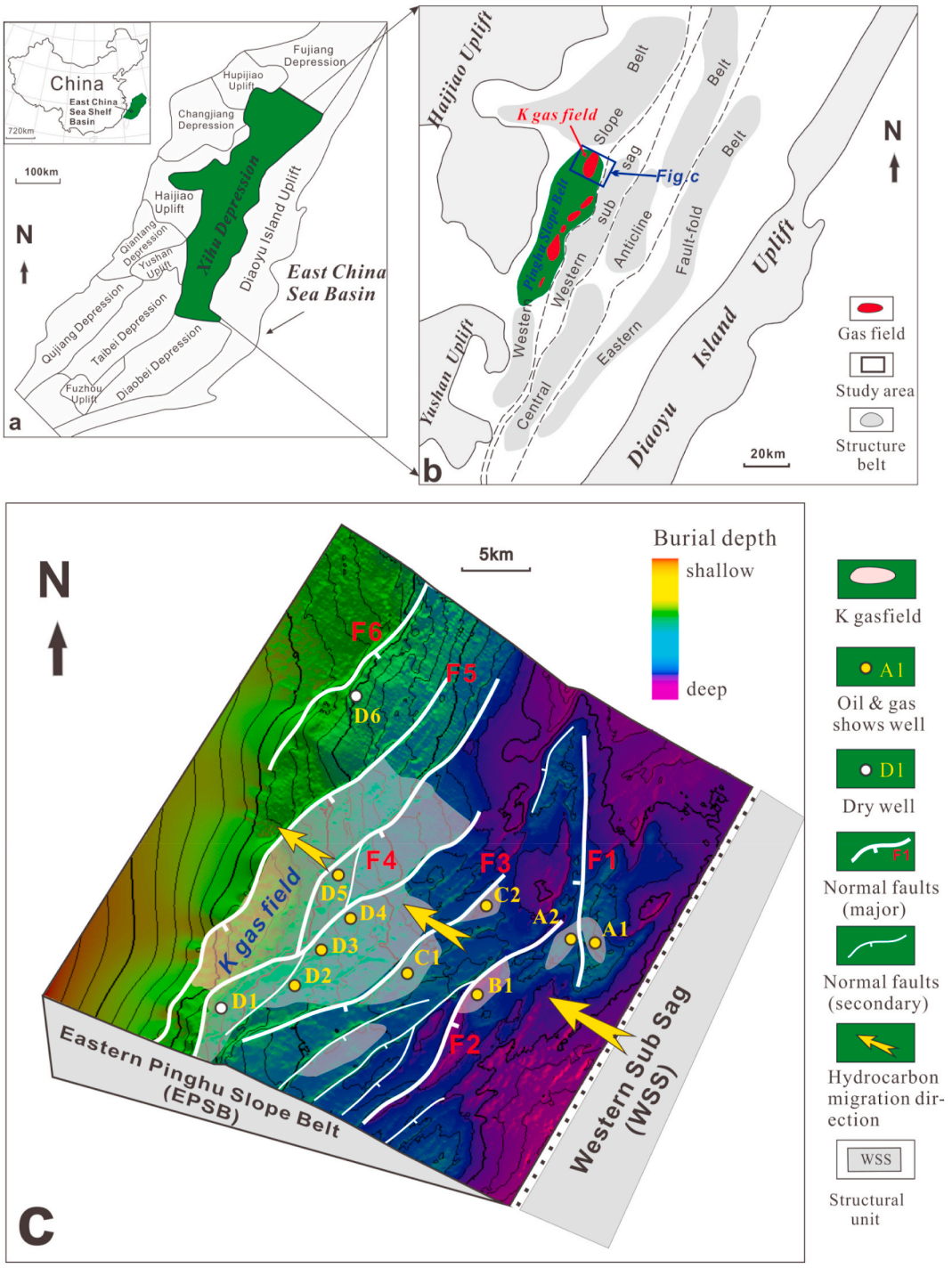

Fig. 1. (a) Map of the East China Sea Shelf Basin; the blue box is the area of the Xihu Depression. (b) Tectonic map of the Xihu Depression showing the location of the Pinghu Slope Belt and main gas fields. The study area is outlined by the box. (c) Structural map of the study area showing the main faults, gas field, drilling wells, and hydrocarbon migration direction. (For interpretation of the references to color in this figure legend, the reader is referred to the Web version of this article.)

Xihu Depression (Xu et al., 2020), and the hydrocarbon accumulations discovered to date are concentrated in the reservoirs of the E_2p and E_3h intervals. This article focuses on the eastern part of the Pinghu Slope Belt (EPSB), where the K gas field that is dominated by fault-controlled traps was discovered (Su et al., 2020). In the study area, the developed normal fault systems are characterized by major NNE-NE trends (Cai and Zhang, 2013; Yang et al., 2014), and the discovered oil and gas are concentrated around the four major fault systems (F1, F2, F3, F4) (Fig. 1c). Moreover, the hydrocarbons that accumulated in faulted anticlines and fault block traps are predominantly natural gas, condensate and light oils (Shan et al., 2015), which charge from the high-to over-mature source rocks of the Western Sub Sag (WSS) and local mature source rocks (Ye et al., 2007; Shan et al., 2015; Zhang et al., 2018; Su et al., 2020). The homogenization temperatures of fluid inclusions indicates that hydrocarbon charging in the study area mainly occurred at 10–3.4 Ma (Shan et al., 2015; Su et al., 2015), which approximately corresponds to the end of the N_1^3l period (Fig. 2). The E_2p source rock with high organic matter in the WSS provided a sufficient gas source and caused large-scale gas washing in the study area (Su et al., 2020). Structural and geochemical tracing analysis has revealed that hydrocarbons generated

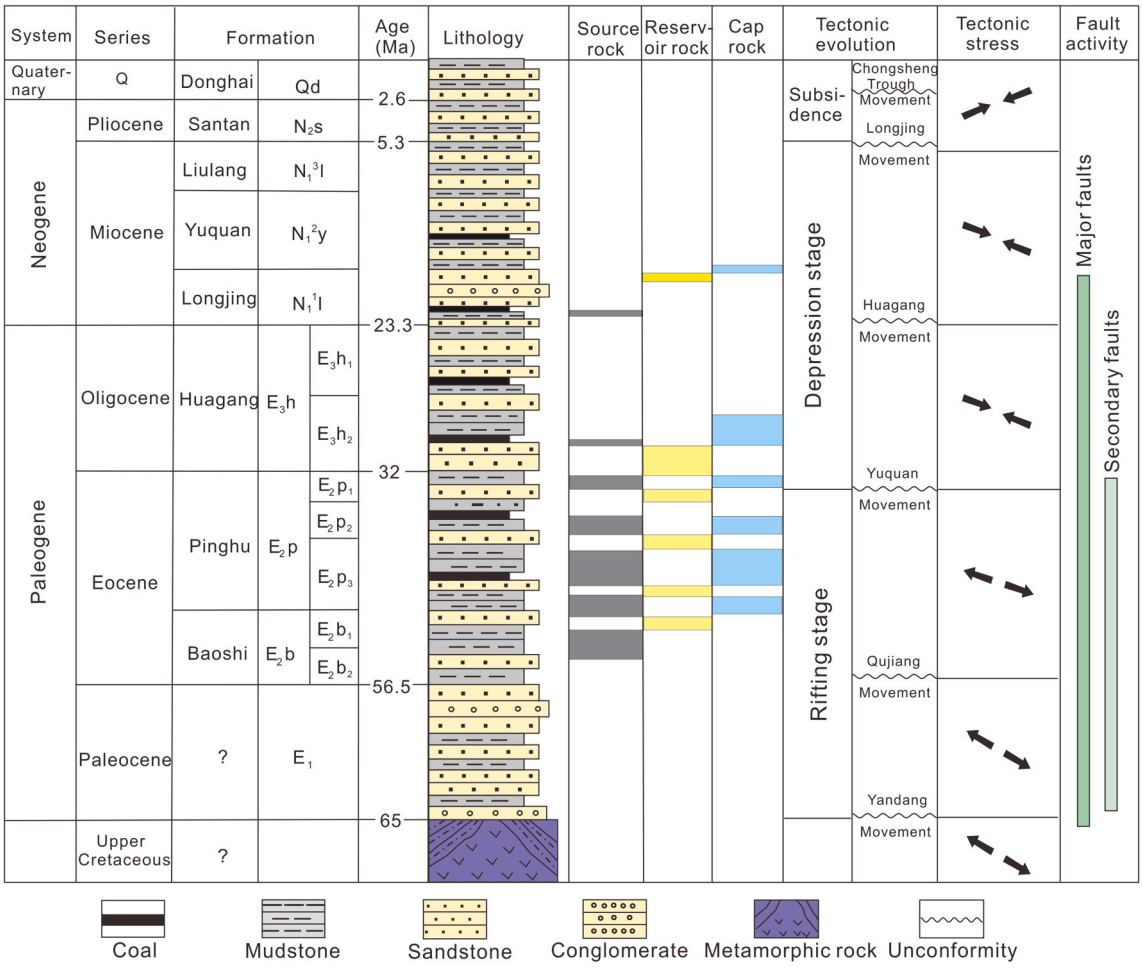

Fig. 2. Summary diagram showing the stratigraphy, tectonic stages, stress direction, and petroleum system in the Xihu Depression (after Su et al., 2020).

from the WSS mainly migrate to the structurally higher positions in the EPSB along the NW direction (Su et al., 2015) (Fig. 1c). For this reason, the four major fault systems (F1, F2, F3, and F4) are all located in the lateral hydrocarbon migration direction, and their strikes are nearly perpendicular to the migration direction.

3. Data and methodology

3.1. Seismic, well logging, pore pressure and vitrinite reflectance data

A high-resolution 3D seismic volume with a dominant frequency of 60 Hz was interpreted to reveal the plane and vertical characteristics of the faults. A total of seven seismic interpretation horizons (T24, T25, T30, T32, T34, T35, and T40) and twenty-four 2D seismic interpretation profiles were used to determine the azimuths, displacements and dip angles of faults. To analyze the hydrocarbon charging conditions along major faults, a total of 92 vitrinite reflectance (Ro) data from 6 wells were collected to determine the threshold depth of mature source rocks. Furthermore, two restored 2D seismic cross-sections (A-A′ and B-B′) were used to reveal the burial depth of the source rock during the charging period using the 2D Move software provided by Midland Valley Company. The workflow of the structural restoration started by decompaction correction, and fault effects were removed using an inclined shear algorithm (White et al., 1986); then, the reconstructed horizon was flattened using a restore algorithm. Finally, cross-sections were balanced and restored at the top of the N_1^3l Formation. Moreover, compensation density curves from 11 wells were collected to investigate the stress component arising from overburden. A total of 43 pore pressure data points measured by the drill stem test (DST) and wireline formation test (WFT) were combined with logging curves from 7 wells to analyze the pressure distribution characteristics. Additionally, the lithologic interpretation and acoustic curves of typical wells were collected to analyze the shale content and compressive strength of fault rocks. The above data were collected from the China National Offshore Oil Corporation (CNOOC) Research Institute and the SINOPEC Shanghai Offshore Oil & Gas Company.

3.2. Identifying the fault vertical sealing index (F_{VSI})

As capillary/permeability sealing is the major mechanism for static fault zone to prevent the vertical leakage of hydrocarbons, the petrophysical properties of fault rocks, such as permeability and capillary threshold pressure control the hydrocarbon sealing properties of faults/fault zones (Schowalter, 1979; Fisher and Knipe, 2001; Fisher and Jolley, 2007; Pei et al., 2015). However, due to the faulting deformation process including clay/phyllosilicate smearing, cataclasis, disaggregation and mixing, the fault rock generated by various types of host sediments presents a significantly stronger heterogeneity than the adjacent host rocks (Smith, 1966, 1980; Yielding et al., 1997; Fossen et al., 2007, 2011). Consequently, it is hard to accurately obtain the permeability or capillary threshold pressure of fault rocks to evaluate the vertical sealing capability. Compared with host rock, the fault rock has generally experienced mixing of different host sediments and varying degrees of deformation, resulting in variations in porosity/permeability. Therefore, analyzing the lithological composition and corresponding deformation degree of given fault rock volumes is an effective approach for

investigating fault vertical sealing and establishing a systematic quantitative evaluation method.

3.2.1. Main factors controlling the deformation of fault rock

Fault rock can be regarded as a highly heterogeneous porous media. According to the deformation mechanism of porous media, the effective stress acting on grain skeleton and the mechanical properties of the grain skeleton together determine the deformation behavior and the pore volume variation (Terzaghi, 1923; Biosh, 1959; Li et al., 1999, Hudson and Harrison, 2000; Tian et al., 2003). The effective stress (P_e) acting on the grain skeleton is affected by both the external stress (σ) and internal stress (pore-fluid pressure (P_f)). For a porous medium with given mechanical properties, the increasing effective stress ($P_e = \sigma - P_f$) tends to reduce the pore space and compress the grain volume, showing a positive correlation with the deformation magnitude and pore reduction of the porous media (Fig. 3a). However, for a given effective stress, porous media with different mechanical properties will also exhibit variations in deformation behavior. The compressive strength can be an indicator of the ability of the grain skeleton to resist deformation or damage caused by external forces (Hudson and Harrison, 2000; Tian et al., 2003). For this reason, porous media with low compressive strength are more likely to deformation under the same effective force, resulting in a significant reduction in pore volume and permeability (Fig. 3b). And thus, the compressive strength of grain skeleton has a negative effect on the compression deformation and pore reduction of the porous media (Fig. 3b). In practice, fault rock is a highly complex porous medium, especially in the composition and mechanical properties of the rock skeleton (Fig. 4). The main controlling factors for the deformation of fault rock need to be further determined in combination with its internal heterogeneity.

Theoretically, the effective stress acting on the framework of fault rock predominantly depends on the difference between the external stress and the pore-fluid pressure in the fault rock (Terzaghi, 1923; Biosh, 1959; Li et al., 1999). Owing to the inclination of the fault surface in spatial content, the external stress acting on the fault rock is equivalent to the stress normal to the fault plane (Fig. 4). As for the pore-fluid pressure, due to the isotropic properties of the fluid, the pore pressure in the fault rock can be approximately regarded as the pressure of the adjacent formation at the same burial depth. And thus, ignoring the impact of porosity on the effective stress, the effective stress acting on the fault rock skeleton can be obtained as the difference between the stress normal to the fault plane and the corresponding fluid pressure (Fig. 4). On the other hand, the deformation magnitude of the fault rock is also related to its compressive strength (Chen and Peng, 1994; Hudson and Harrison, 2000; Tian et al., 2003), which refers to the maximum compressive stress that a rock can withstand before it is damaged. Under the same compressive stress conditions, rocks with higher compressive strength are generally more difficult to deform, and therefore, less permeability reduction occurs. Rock mechanics and numerical simulation experiment have indicated that the compressive strength of rock varies with lithology and burial depth (Chen and Peng, 1994; Wang et al., 2005; He et al., 2011). The compressive strength of sandstone is usually greater than that of shale or mudstone. For heterogeneous siliciclastic strata characterized by interbedded shale and sandstone, the fault rock is a mixture of different amounts of sandstone and shale/-mudstone (Fig. 4), so its overall compressive strength may decrease with increasing shale content. Furthermore, due to the confining pressure varies with the buried depth, the rock compressive strength is usually positively correlated with burial depth (Chen and Peng, 1994; Wang et al., 2005). Overall, the stress normal to the fault plane, the pore-fluid

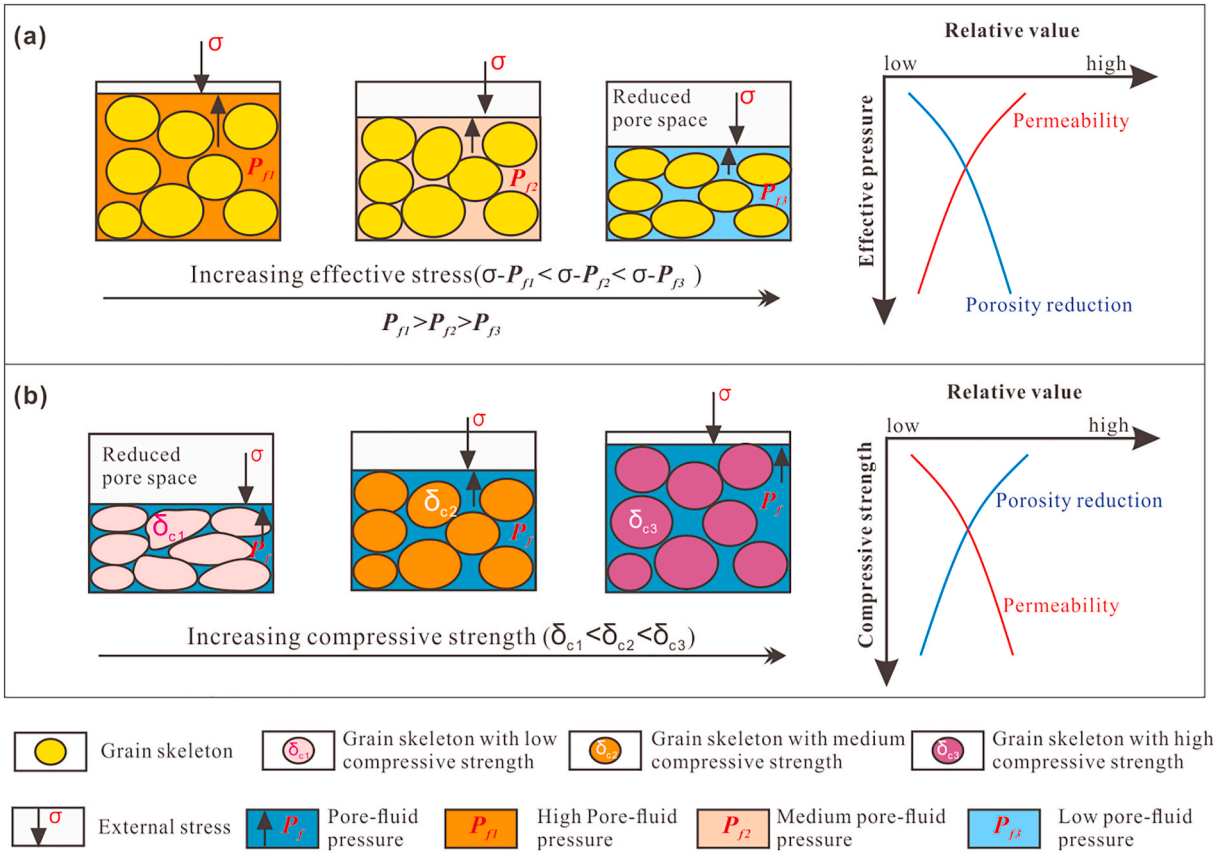

Fig. 3. Conceptual diagram showing the control of the effective stress and compressive strength of the grain skeleton on porous media deformation; (a) A conceptual model showing the deformation, porosity and permeability characteristics of the same porous media with increasing effective stress; (b) The deformation, porosity and permeability variations of the porous media with different compressive strengths under the same effective stress.

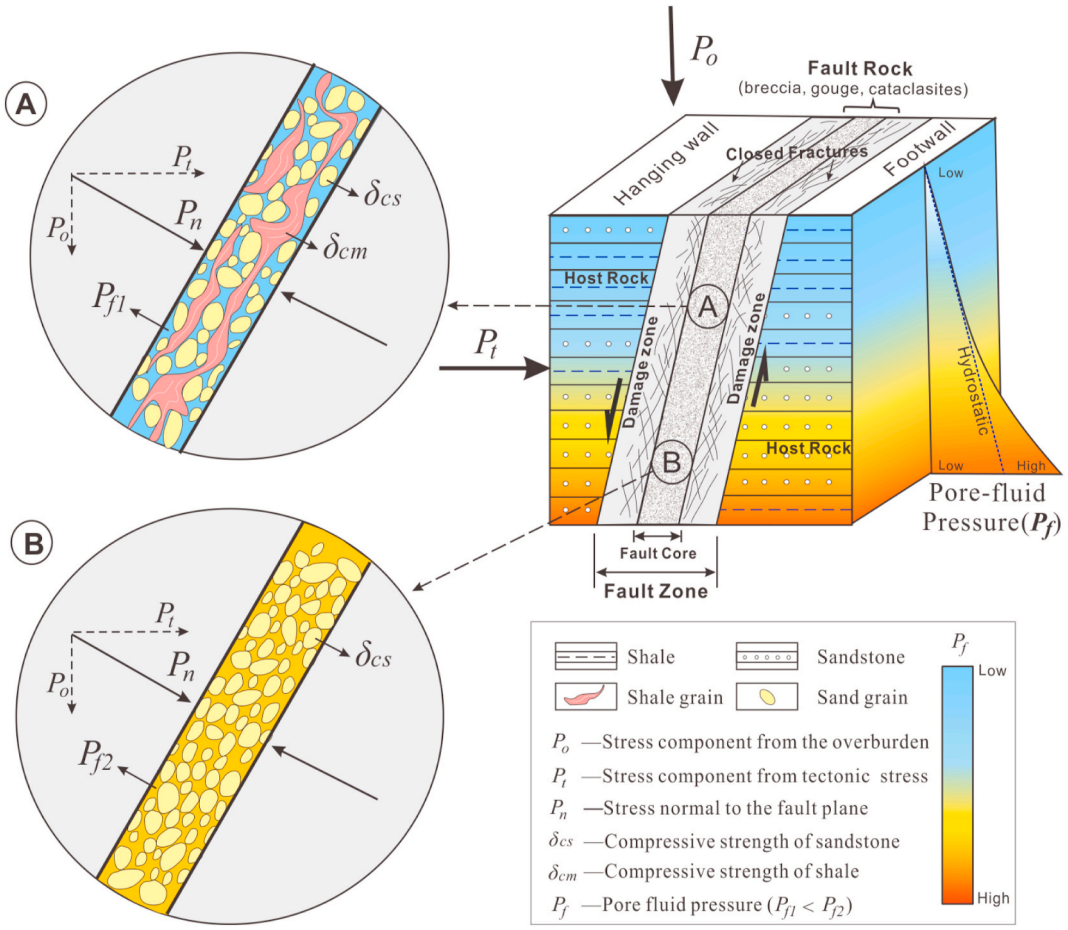

Fig. 4. Conceptual diagram showing the control of the stress normal to the fault plane ($\boldsymbol{P_n}$), pore fluid pressure ($\boldsymbol{P_f}$) and rock compressive strength ($\boldsymbol{\delta_c}$) on fault rock deformation. Different fault rocks are generated when various types of host rocks are entrained into the fault zones during faulting processes, and it is mainly distributed within the fault core and includes fault gouge, breccias, and cataclasites, etc. A reflects fault rocks with high mudstone content under hydrostatic pressure ($\boldsymbol{P_{f1}}$), and B indicates fault rocks without mudstone smears under overpressure ($\boldsymbol{P_{f2}}$). $\mathbf{P_n}$ is derived from the stress component from the overburden ($\boldsymbol{P_o}$) and the regional tectonic stress ($\boldsymbol{P_t}$). The $\boldsymbol{\delta_c}$ of fault rock is determined by the compressive strength of mudstone/shale ($\boldsymbol{\delta_{cm}}$) and sandstone ($\boldsymbol{\delta_{cs}}$) inside the fault rock. Since $\boldsymbol{\delta_{cm}}$ is usually less than $\boldsymbol{\delta_{cs}}$, the $\boldsymbol{\delta_c}$ value of fault rock decreases with increasing mudstone content. Under the same $\boldsymbol{P_n}$ condition, the fault rock in A is more easily deformed than that in B due to the larger effective stress and smaller compressive strength.

pressure and the compressive strength of the fault rock controlled by the buried depth and shale content can be identified as the three main factors affecting fault rock deformation.

3.2.2. *Definition of fault vertical sealing index (F_{VSI})*

The vertical sealing capacity of static fault zone predominantly depends on the petrophysical properties of fault rock. As the compression deformation magnitude of the fault rock is positively correlated with the porosity/permeability reduction (Figs. 3 and 4), the parameters reflecting the deformation of fault rock can be used to evaluate the capillary seal difference of fault zones. Recent studies have indicated the role of individual factors involving stress normal to the fault plane, pore-fluid pressure and rock compressive strength in the fault zone sealing capability by permeability/capillary seal. However, due to the difficulty of quantifying the compressive strength of fault rocks, these three different factors have only rarely been integrated to comprehensively analyze the hydrocarbon sealing properties of the faults. To obtain a more accurate quantitative evaluation of fault vertical sealing, we have established a method for estimating the compressive strength of fault rocks based on shale content analysis and well logging calculations. Furthermore, we incorporated pore-fluid pressure, normal stress and rock compressive strength together by using fault rock deformation as a link, and propose a new composite parameter of the "fault vertical sealing index", expressed as F_{VSI}. Considering the main factors that cause the porosity/permeability of fault rocks to change, the F_{VSI} is defined as the ratio between factors favoring fault vertical sealing (reducing permeability), represented by the effective stress acting on the fault rock (P_e), and factors promoting fault vertical non-sealing (enhancing or maintaining permeability), represented by compressive strength of fault rock (δ_c), as written in Eq. (1). The increasing P_e is positively correlated with the compression deformation magnitude and pore reduction of the fault rock, and the resulting diminish in permeability is conducive to enhancing the sealing ability (Figs. 3 and 4). The P_e can be obtained by the difference between the stress normal to the fault plane (P_n) and the corresponding pore-fluid pressure (P_f). Conversely, the increasing δ_c is beneficial to resist compression deformation of fault rock and maintain permeability, which is negatively related to the capillary sealing ability (Figs. 3 and 4). The compressive strength of fault rock varies with composition (shale/mudstone content) and burial depth, and the detailed acquisition approach will be illustrated in the following section. In this way, the values of F_{VSI} can be calculated from the values of these three independent parameters, a larger value of F_{VSI} indicates the more fault rock compression deformation, permeability (porosity) reduction, and therefore the stronger capillary/permeability sealing of the heterogeneous fault zone.

$$F_{VSI} = \frac{P_e}{\delta_c} = \frac{P_n - P_f}{\delta_c} \quad (1)$$

where F_{VSI} is the fault vertical sealing index, which is dimensionless; P_e is the effective stress acting on the fault rock in MPa; δ_c is the compressive strength of the fault rock in MPa; P_n is the stress normal to the fault plane in MPa; and P_f is the pore fluid pressure in MPa.

This method can be used to quantitatively describe the changes of vertical permeability seal caused by the magnitude of fault rock deformation. However, fault seal analysis based on the prediction of fault rock deformation can be biased if cemented fault zones are extensively developed (Knipe, 1993a; Knipe et al., 1997; Jolley et al., 2007b; Pei et al., 2015). Cementation is another mechanism of the permeability reduction within fault zone except for the fault rocks deformation caused by compaction (Knipe et al., 1997). However, the cement seals are mostly associated with the sites where local minerals dissolution and reprecipitation happen during deformation or along the invasion paths of fluids in the faults. In most cases, the cementation can rarely form continuous seals and is often restricted to limited areas of the fault zone (Ottesen Ellevset et al., 1998). Additionally, cementation is difficult to quantitatively use for sealing evaluation, as the cementation properties are hard to obtain and varies within a big range. For this reason, this article adopts the fault sealing index (F_{VSI}) without considering the cementation effect to characterize the vertical sealing of the major fault systems.

3.3. Quantitative characterization of evaluation parameters

3.3.1. Stress normal to the fault plane (P_n)

As the principal source of effective stress on the fault rock, the stress normal to the fault plane (P_n) should be positively correlated with the vertical sealing capability of the fault zone. The normal stress component on a fault plane arises from the weight of the overburden sediment and the regional tectonic stress (Lü et al., 1996; Fu et al., 1997), which can be expressed as Eq. (2). The key to calculating the stress component from the overburden (P_o) is the acquisition of the fault dip angle (α) and formation density (ρ_b). The value of α can be measured by the seismic interpretation profile shown in Fig. 5a, and the formation density (ρ_b) at different locations can be obtained through the density variation model with burial depth, as shown in Fig. 5c and Eq. (3). According to the borehole breakout and numerical simulation results, the direction of the regional tectonic principal stress (δ) during the Pliocene-Quaternary period is NEE-SWW (approximately 65°) (Xu and Wu, 1997; Xu et al., 1999; Zhang et al., 2002). The model of horizontal tectonic principle stress variation with burial depth is obtained by fitting the measured stress data of the nearest area (Xu and Wu, 1996), as shown in Fig. 5d and Eq. (4). Eqs. (2)–(4) are shown as follows:

$$P_n = P_o + P_t = H(\rho_b - \rho_w) * 0.009876 cos\alpha + \delta sin\beta sin\alpha \quad (2)$$

$$\rho_b = 0.43 \ln(H) - 1.08 \quad (R^2 = 0.64) \quad (3)$$

$$\delta = 0.024H - 5.75 \quad (R^2 = 0.85) \quad (4)$$

where P_n is the stress normal to the fault plane (MPa), P_o is the stress component from the overburden (MPa), P_t is the compressive tectonic stress component (MPa), H is the burial depth (m), ρ_b and ρ_w are the densities of overburden sediments and formation water (g/cm^3), respectively, α is the fault dip angle (°), δ is the horizontal tectonic principal stress (MPa), and β is the intersection angle between the direction of the tectonic stress and fault strike, which can be determined by the fault polygon interpretation shown in Fig. 5b.

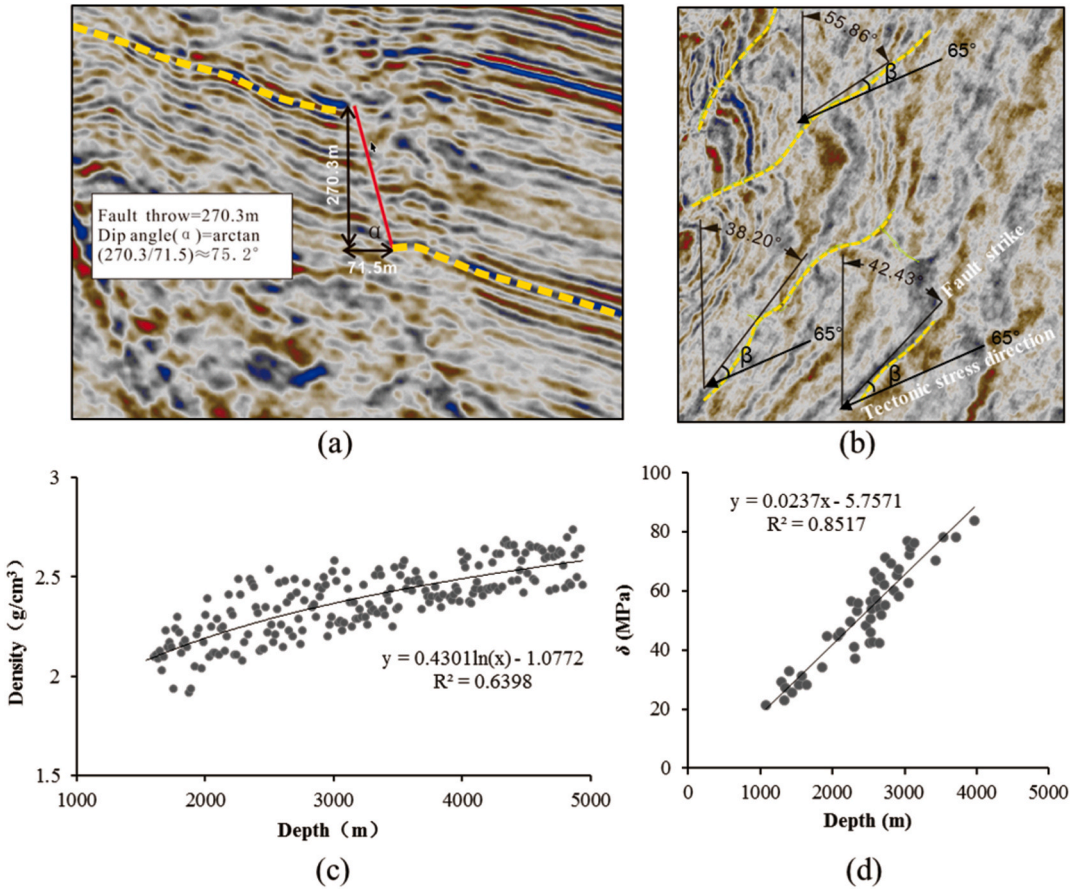

Fig. 5. (a) An example of measuring the fault throw and dip angle (α). (b) An example of measuring the intersection angle between the direction of the tectonic stress and fault strike. (c) Model of overburden sediment density varying with burial depth. (d) Model of regional horizontal tectonic principle stress varying with burial depth (Xu and Wu, 1996).

3.3.2. Pore-fluid pressure (P_f)

Since the pore-fluid pressure exerts a stress opposite to the effective stress (Fig. 4), the mechanical strength and effective stress component of fault rock decrease with increasing pore-fluid pressure (Hubbert and Rubey, 1959; Jaeger and Cook, 1979; Byerlee, 1993; Luo, 2004), resulting in a negative correlation between fault vertical sealing and pore-fluid pressure. Due to the isotropic properties of the fluid, the pore-fluid pressure of the fault rock can be approximately regarded as the adjacent formation pressure at the same burial depth. Since the measured pressure data are scarce and difficult to obtain, the current measured pore pressures (from the drill stem test and wireline formation test) cannot meet the evaluation requirements at different burial intervals. Well log data (measured as sonic travel time) are an efficient dataset for continuous pressure observation by using the equivalent depth method (Hottman and Johnson, 1965; Magara, 1968; Webster et al., 2011), as shown in Fig. 6. In this study, a total of 43 measured data and acoustic logs from 7 drilling wells are combined to estimate the pore-fluid pressure of fault rocks at different depths.

3.3.3. Shale content and compressive strength of fault rock (δ_c)

The compressive strength of rock varies greatly with lithology and burial depth (Chen and Peng, 1994; Wang et al., 2005; He et al., 2011). The compressive strength of sandstone is usually greater than that of shale or mudstone. For the strata characterized by interbedded shale and sandstone, the fault rock is a mixture of different amounts of sandstone and shale/mudstone. For heterogeneous siliciclastic strata, the amount of shale entrained into the fault zone during the faulting process can be estimated using the shale gouge ratio (SGR) (Yielding et al., 1997), as shown in equation (5):

$$\mathrm{SGR} = \frac{\sum \text{shale bed thickness}}{\text{fault throw}} \times 100\% \quad \text{or}$$
$$\mathrm{SGR} = \frac{\sum[(\text{Zone thickness}) \times (\text{Zone shale fraction})]}{\text{fault throw}} \times 100\% \tag{5}$$

Under the same effective stress conditions, the overall compressive strength of the fault rock decreases with increasing shale content. In previous evaluation studies, the compressive strength of sandstone and mudstone were generally regarded as fixed values (Tian et al., 2003; Li et al., 2020). However, recent experimental and simulation data have shown that rock compressive strength is usually positively correlated with burial depth (Chen and Peng, 1994; Wang et al., 2005), where the confining pressure is different. In practice, core samples of overburden formations used for laboratory tests are scarce and difficult to obtain. Hence, it is difficult to observe variations in compressive strength at different depths with limited measurement data. Since many factors that affect the rock compressive strength also impact other petrophysical properties, a variety of empirical relations have been proposed to relate the rock compressive strength to parameters such as porosity, velocity, and elastic moduli that can be measured by well logs (Chang et al., 2006). In this study, the commonly available sonic transit time (Δt) data are used to estimate the rock compressive strength. The compressive strength of shale (δ_{cm}) is estimated according to the empirical relationship given by Horsrud (2001), as shown in equation (6). The compressive strength of sandstone (δ_{cs}) is determined by the empirical relationship proposed by McNally et al. (1987) on the basis of sandstone laboratory test data, as expressed in equation (7). The good match between the measured data collected from adjacent areas (Sun et al., 2016) and the predicted results at different depths indicates the applicability of the method of empirical relations in the study area, as shown in Fig. 7. Equations (6) and (7) are shown as follows:

$$\delta_{cm} = 0.77\left(\frac{304.8}{\Delta t}\right)2.93 \tag{6}$$

$$\delta_{cs} = 1200exp(-0.036\Delta t) \tag{7}$$

where δ_{cm} is the compressive strength of shale (MPa), Δt is the sonic transit time (μs/ft), and δ_{cs} is the compressive strength of sandstone (MPa).

Therefore, based on the compressive strength estimated from acoustic logs, the relation between the compressive strength and depth of each well can be further established. Using Well B1 as an example, the functions describing mudstone and sandstone compressive strengths with depth are given in equations (8) and (9), respectively. Thus, when the fault rock is approximately regarded as a mixture of shale and

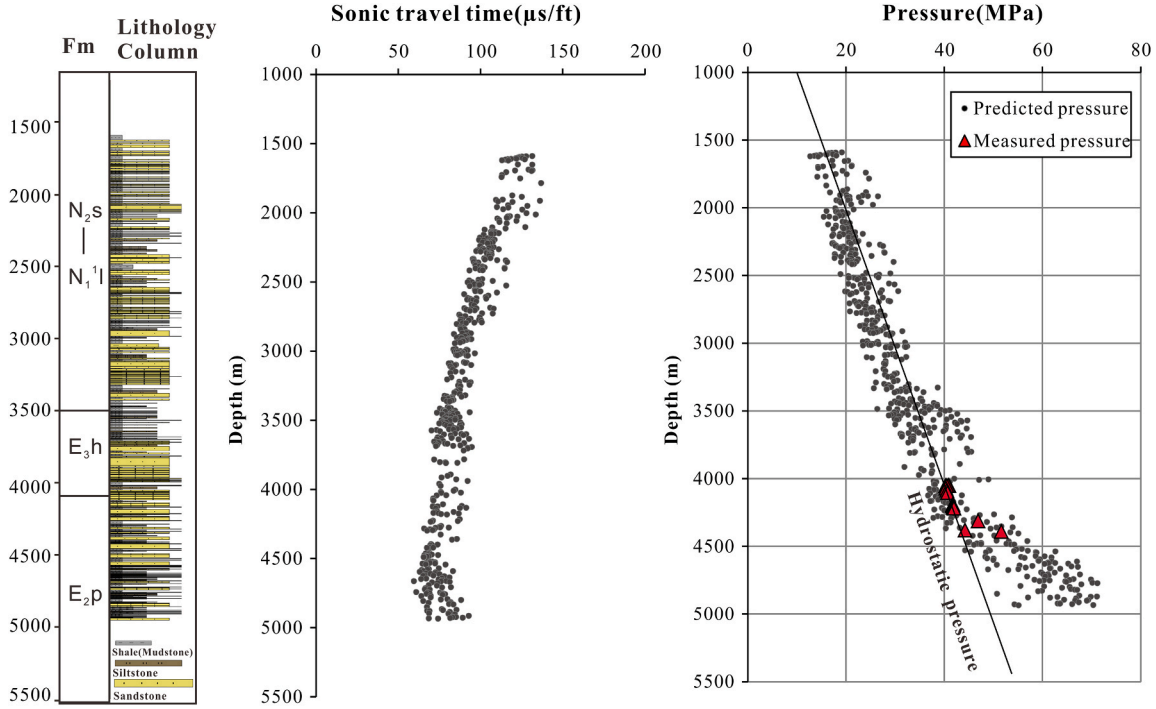

Fig. 6. Lithologic column, well log curve (sonic travel time), drill stem test data (DST), and corresponding predicted pressure in Well B1 from the K gas field.

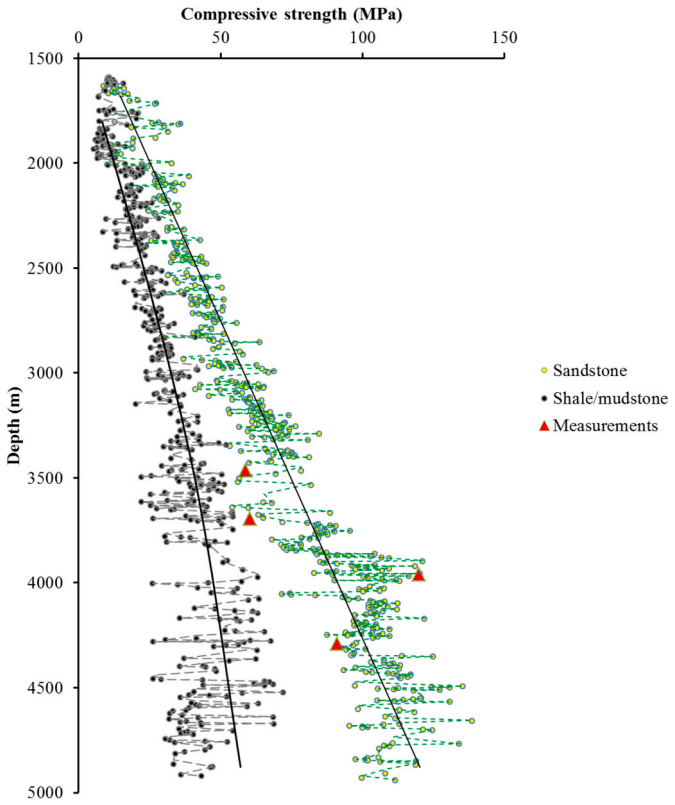

Fig. 7. Prediction results of the compressive strength of mudstone and sandstone in Well B1 based on the acoustic curve. The red triangle represents the measured sandstone compressive strength data collected in the Xihu Depression (Sun et al., 2016). (For interpretation of the references to color in this figure legend, the reader is referred to the Web version of this article.)

sandstone at the same depth, the compressive strength of fault rocks with different shale contents can be estimated by equation (10). Equations (8)-(10) are shown as follows:

$$\delta_{cmh} = 39.458ln(H) - 284.23 \quad (R^2 = 0.7241) \tag{8}$$

$$\delta_{csh} = 0.0346H - 46.080 \quad (R^2 = 0.92) \tag{9}$$

$$\delta_c = SGR * \delta_{cmh} + (1 - SGR) * \delta_{csh} \tag{10}$$

where δ_{cmh} is the compressive strength of shale varying with burial depth (MPa), H is the burial depth of rock (m), δ_{csh} is the compressive strength of sandstone varying with burial depth (MPa), δ_c is the compressive strength of fault rock (MPa), and SGR is the shale gouge ratio of fault rock.

4. Results

4.1. Spatial geometric characteristics of faults

4.1.1. Plane geometric characteristics of faults

Plane views of fault polygons interpreted from 3D seismic data are shown in Fig. 8. The fault systems developed in the EPSB are composed of a series of N-, NNE- and NE-striking faults, with a dominance of NNE- and NE-striking trends. There are six major faults extending laterally over long distances, the faults of F2, F3, F4, F5, and F6 are NE-striking stepped normal faults accompanied by arc-shaped secondary faults with NNE- and NE-striking trends, whereas the F1 is a NNE-striking normal fault with NE-striking secondary faults. According to the fault strike azimuth frequency distribution, the orientations of the faults are mainly 40°–50° (Fig. 9), and the strike azimuth varies in different parts of the faults. Based on the regional tectonic stress orientation, the intersection angles between the fault strikes and tectonic stress are distributed between 5° and 105° (Figs. 8 and 9), which will result in the variation in stress normal to the fault plane.

4.1.2. Vertical geometric characteristics of faults

The 2D seismic profiles were interpreted to analyze the vertical characteristics of faults. As shown in Fig. 10, the normal fault systems in the study area present two different dipping directions, and the dip angles are mostly between 60° and 75°. The F2, F3, F4, F5, and F6 fault systems located in structurally higher positions are characterized by the same dip orientations as those of the strata, while the structurally lower F1 fault and its adjacent secondary faults are opposite to the strata dipping tendency. In terms of geometric shape, the major faults are all listric growth faults whose dip angle decreases with burial depth, whereas the accompanying and isolated secondary faults are mostly flat faults. Moreover, the six major faults spatially connect the E_2b, E_2p and E_3h Formations, while most of the secondary faults only extend upward to the E_2p Formation. Nevertheless, the activity of six major faults occurred before the hydrocarbon charging period and generally ceased after deposition of the E_3h Formation (Fig. 11).

4.2. F_{VSI} distribution characteristics of major faults

Combined with the evaluation of stress normal to the fault plane (P_n), pore-fluid pressure (P_f), and fault rock compressive strength (δ_c), the fault vertical sealing index (F_{VSI}) of four major faults related to hydrocarbon distribution (F1, F2, F3, and F4) in the EPSB is evaluated. The F_{VSI} value varies greatly with different faults and presents a heterogeneous distribution on each fault plane.

4.2.1. F_{VSI} distribution characteristics of fault F1

For the F1 fault system, the stress normal to the fault plane (P_n) increases with burial depth and decreases slightly from the central fault to both sides (Fig. 12a). As shown in Fig. 12b, the pore-fluid pressure (P_f) above 4200 m is characterized by a gradual increase in hydrostatic conditions, followed by a sharp increase, indicating the presence of overpressure. The heterogeneous SGR on the fault plane indicates that the fault rocks in the depth intervals of 3700–4100 m have relatively high shale contents (Fig. 12c). Conversely, the fault rocks with high compressive strength estimated based on the SGR are concentrated in depth intervals of 4200–4700 m (Fig. 12d). Finally, the F_{VSI} evaluation was obtained by integrating the above parameters. On fault F1, relatively high F_{VSI} values appear in the burial interval of 3500–4300 m, indicating strong vertical sealing. In contrast, the fault rock with burial depths below 4300 m is characterized by weaker vertical sealing (Fig. 12e).

4.2.2. F_{VSI} distribution characteristics of fault F2

As shown in Fig. 13a, the stress normal to the F2 fault plane increases with burial depth. Meanwhile, due to the variation in the intersection angle between the fault strike and the tectonic stress, the normal stress in the western part of the fault is slightly stronger than that in the eastern part. For the pore-fluid pressure, the rapid increase in pressure below 4300 m suggests the presence of overpressure (Fig. 13b). The distribution of the SGR on the fault plane shows strong nonuniformity due to the disparity in the fault displacement and faulting lithology at different locations. There are three relatively high SGR distributions in the depth intervals of 3500–3800, 4300–4700, and 4800–5000 m (Fig. 13c). The compressive strength of fault rock (δ_c) estimated based on the SGR is shown in Fig. 13d, where the relatively high δ_c areas are concentrated in depth intervals of 3900–4300 m and 4700–4800 m. On fault F2, there are three relatively high F_{VSI} distributions in the depth intervals of 3500–3900 m, 4000–4700 m, and 4800–4900 m (Fig. 13e). Among them, the largest F_{VSI} value appears within the interval of 3500–3900 m,

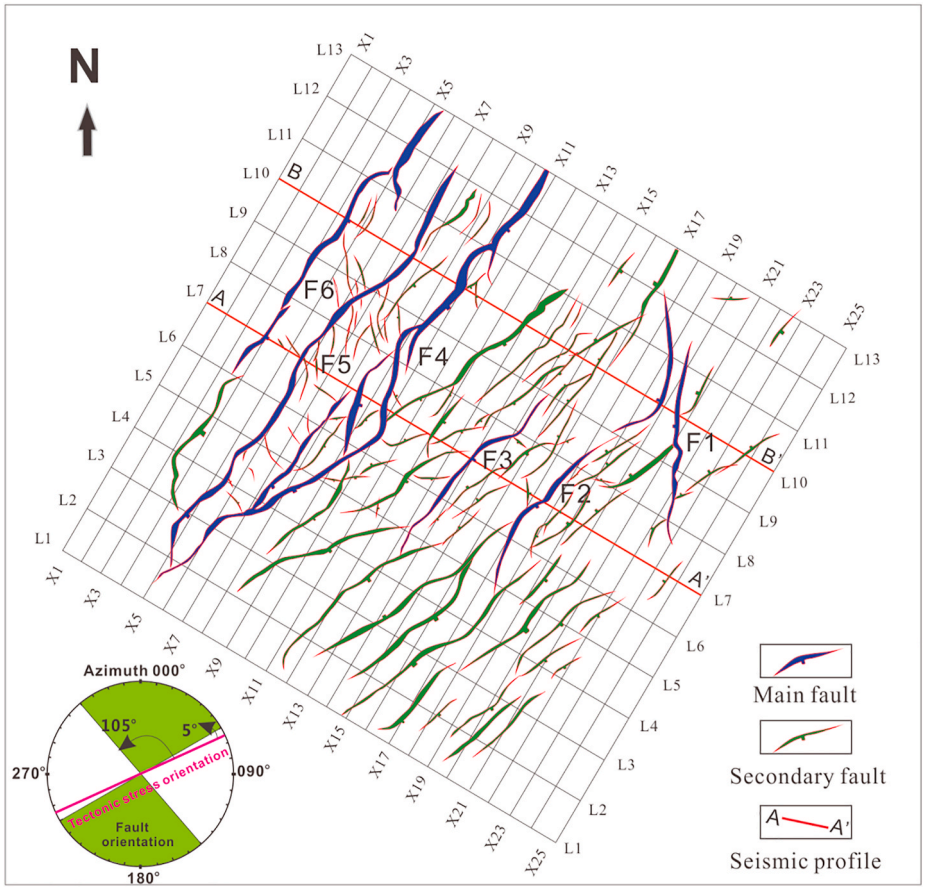

Fig. 8. Plane geometric characteristics of fault polygons based on 3D seismic interpretation of T32 horizon in the eastern Pinghu Slope Belt. See Fig. 9 for the locations of T32 horizon.

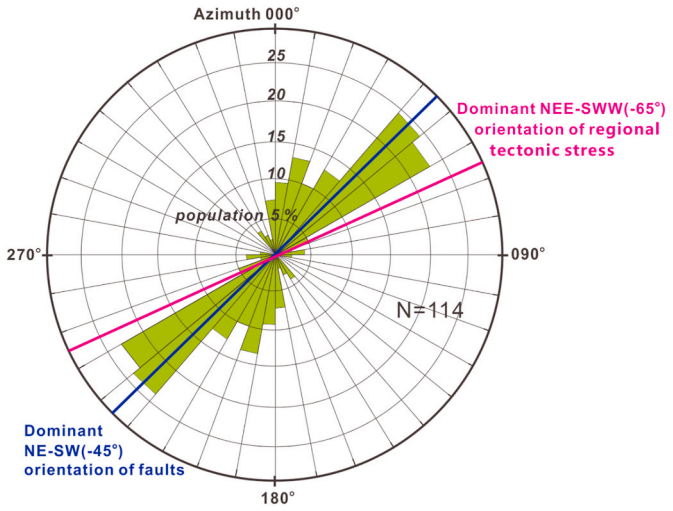

Fig. 9. Fault strike azimuth frequency distribution in the eastern Pinghu Slope Belt. The solid blue line indicates the dominant orientation of faults, and the solid red line indicates the dominant orientation of regional tectonic stress. (For interpretation of the references to color in this figure legend, the reader is referred to the Web version of this article.)

indicating strong vertical sealing.

4.2.3. F_{VSI} distribution characteristics of fault F3

For the F3 fault system, the stress normal to the fault plane increases with burial depth and shows a slight decrease from the western part to the eastern part of the fault (Fig. 14a). For the pore-fluid pressure, slight overpressure characteristics appear below 4200 m (Fig. 14b). The heterogeneous SGR on the fault plane indicates that the fault rocks in the depth intervals of 3000–3500 m, 3700-410 m, and 4300–5000 m have relatively high shale contents (Fig. 14c). However, the relatively high compressive strength of the fault rock (δ_c) controlled by the burial depth and shale content is concentrated in depth intervals of 3400–3800 m, 4100–4300 m and 4600–5000 m (Fig. 14d). On fault F3, there are three relatively high F_{VSI} distributions in the depth intervals of 3200–3300 m, 3800–4100 m, and 4200–4500 m, indicating strong vertical sealing (Fig. 14e). Generally, the vertical sealing of the western part of the fault is stronger than that of the eastern part.

4.2.4. F_{VSI} distribution characteristics of fault F4

For the F4 fault system, the stress normal to the fault plane increases with burial depth and shows an increase from the western part to the eastern part of the fault (Fig. 15a). For the pore-fluid pressure, the western part of the fault is characterized by hydrostatic pressure, while the eastern part of the fault shows overpressure below 4350 m (Fig. 15b). As shown in Fig. 15c, the two relatively high SGR areas are mainly distributed in the depth interval of 2600–3000 m in the E_3h Formation and 3200–4000 m in the E_2p Formation. In addition, the compressive strength of the F4 fault rock is generally lower than that of other faults because of the shallow burial depth and high shale content (Fig. 15d). The areas with high compressive strength are mainly distributed below 3800 m in the eastern part of the fault. In this fault, the eastern part of the fault shows relatively high F_{VSI} values (>0.6) at depth intervals of 3400–4600, while the F_{VSI} values displayed in the western part are mostly less than 0.6. Overall, the vertical sealing capability of the eastern part of the fault is obviously stronger than that of the western

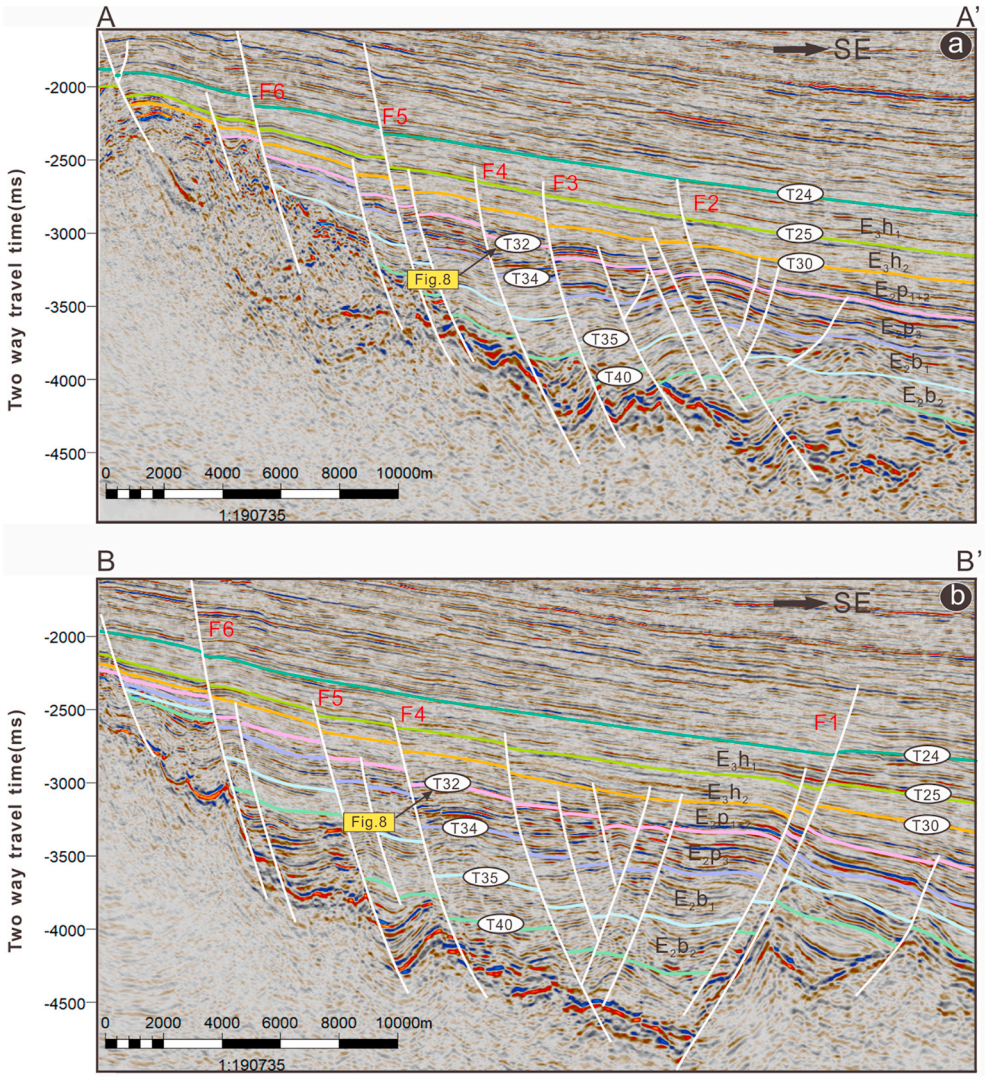

Fig. 10. Vertical geometric characteristics of faults based on 2D seismic interpretation sections. See Fig. 8 for the locations of AA′ and BB′ profiles.

part (Fig. 15e).

4.3. Hydrocarbon distribution and charging condition along faults

Although the faults F1, F2, F3, and F4 have spatially connected the source rocks and the reservoirs within the E_2b, E_2p, and E_3h Formations, the vertical hydrocarbon distribution along the faults presents great differences (Fig. 16). For the hydrocarbon accumulation related to faults F2, F3, and F4, the discovered natural gas and oil are characterized by being concentrated in the reservoir within the E_2p Formation, except for the small amount of gas accumulated in the E_2h Formation of Wells B1 and C2. However, the accumulation of natural gas near the F1 fault presents a vertical multilayer distribution in the reservoir of the E_2p and E_3h Formations (Fig. 16), which demonstrates the occurrence of vertical hydrocarbon migration along the fault.

The faults at different locations have a variation in hydrocarbon charging conditions. The hydrocarbons accumulated in fault anticlines and fault block traps in the EPSB are charged by hydrocarbons generated from the high-to over-mature source rocks of the Western Sub Sag (WSS) and local mature source rocks. The F1, F2, F3, and F4 faults are sequentially distributed in the direction of lateral hydrocarbon migration, as the distance increases, the hydrocarbon charging from WSS gradually weakens. However, for local hydrocarbon charging, only mature source rocks can provide oil and gas sources for connected faults during the charging period. The relationship between vitrinite reflectance (Ro) and burial depth indicates that the source rock enters the mature stage of hydrocarbon generation at a burial depth of 2800 m (Fig. 17a). To determine the local charging conditions, the seismic cross-sections AA′ and BB’ were balanced and restored at the top of the N_1^3l Formation using 2D Move software to obtain the burial depth of the source rock during the charging period. As shown in Fig. 17b and c, the F1 and F2 faults located in the structurally lower position are connected with local mature source rocks, indicating that there could be a local hydrocarbon charge, whereas the immature source rocks distributed in the structurally higher position cannot provide hydrocarbon sources for faults F3 and F4 during the main charging period. For this reason, the F1 and F2 faults may have both local vertical and WSS lateral hydrocarbon charging, whereas the hydrocarbons near F3 and F4 only come from the lateral hydrocarbon charging of the sand bodies along the structurally lower position.

5. Discussion

As effective vertical conduits for fluid flow, faults affect the migration, accumulation and, therefore, the distribution of hydrocarbons. In most cases, the faults connecting mature source rocks and favorable reservoirs are expected to provide potential pathways for vertical hydrocarbon migration. On the other hand, hydrocarbons that migrate

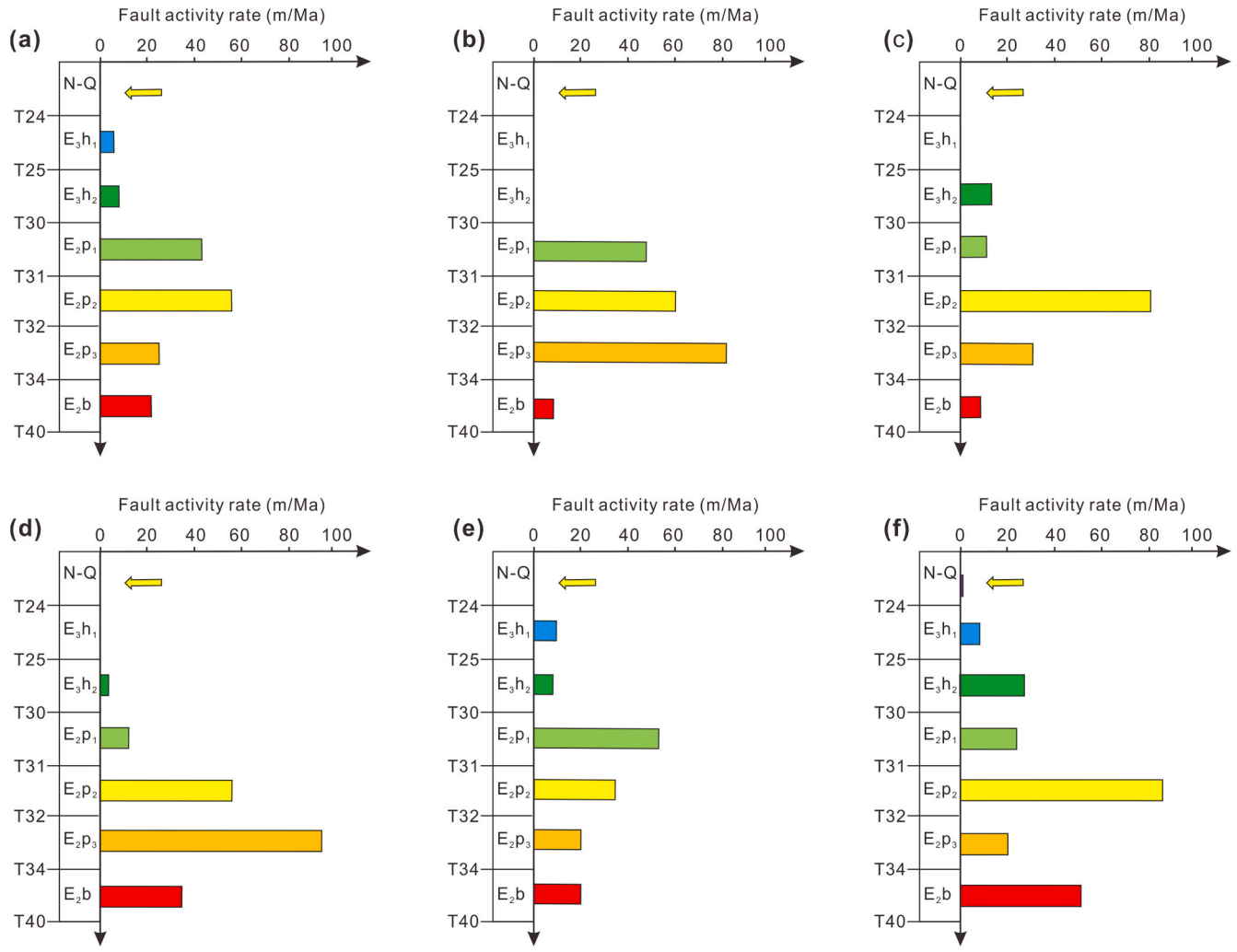

Fig. 11. (a), (b), (c), (d), (e) and (f) show the fault activity rates of the F1, F2, F3, F4, F5 and F6 faults, respectively. The fault activity rate is defined as the ratio of the thickness difference between the strata on the hanging wall and the footwall to the corresponding deposition duration. The yellow arrow indicates the main hydrocarbon charging period determined by the homogenization temperatures of fluid inclusions (oil and aqueous fluid) (Su et al., 2015). (For interpretation of the references to color in this figure legend, the reader is referred to the Web version of this article.)

laterally along connected sand bodies may continue to migrate vertically when encountering vertical unsealed faults. During the hydrocarbon charging, active faults are commonly opened and act as vertical conduits for fluid flow controlled by "seismic pumping" (Sibson et al., 1975; Blair and Bilodeau, 1998; Eichhubl and Boles, 2000; Hao et al., 2009; Indrevær et al., 2014). In the EPSB, due to the hydrocarbon charging time (Pliocene) determined by fluid inclusions is greatly later than the duration of fault movement (Paleogene) (Zhang, 2013; Shan et al., 2015) (Fig. 11), the vertical differential distribution of hydrocarbons is most likely related to the vertical sealing of static faults. Quantitative evaluations of the fault vertical sealing index (F_{VSI}) can reflect the capability of the fault zone to seal or transport hydrocarbons during the quiescent period. However, the concrete relations between vertical sealing and the process of hydrocarbon migration and accumulation need to be further analyzed based on the charging situation and distribution characteristics of hydrocarbons.

5.1. The relations between the F_{VSI} and hydrocarbon distribution

For inactive faults during the hydrocarbon charging, vertical sealing capacity plays an important role in the processes of hydrocarbon migration and accumulation. Theoretically, weakly sealed faults are easier to serve as conduits for vertical hydrocarbon migration, while strongly sealed faults are generally acted as permeability barriers to hydrocarbon accumulation. However, a fault cannot be uniformly regarded as a conduit or a barrier because the vertical sealing properties of the fault zone vary everywhere. The heterogeneous F_{VSI} distribution confirms that fault vertical sealing changes along different positions (Figs. 12–15), which may result in complex processes of hydrocarbon migration and accumulation. Under the control of buoyancy, natural gas or oil always preferentially migrates upwards. And thus, fault vertical sealing is the principal prerequisite for hydrocarbon accumulation, although it is also controlled by lateral sealing. For this reason, the current hydrocarbon accumulation characteristics can provide an indication of the vertical sealing capacity of a fault. In this article, the F_{VSI} value of the fault zone and the corresponding oil and gas shows reveal that there are three relations between fault vertical sealing and hydrocarbon migration and accumulation behavior.

For the first case, when the F_{VSI} value is lower than a certain value, the fault zone completely acts as a vertical conduit and cannot seal hydrocarbons. Using the F3 fault as an example, the F_{VSI} values displayed in the eastern part of the F3 fault are mostly less than 0.5 (Fig. 14), indicating a weak vertical sealing ability. As a result, the hydrocarbons that migrated laterally from the structurally lower positions continued to migrate upwards along the fault zone to the E_3h Formation, and the hydrocarbons present in Well C2 support this interpretation

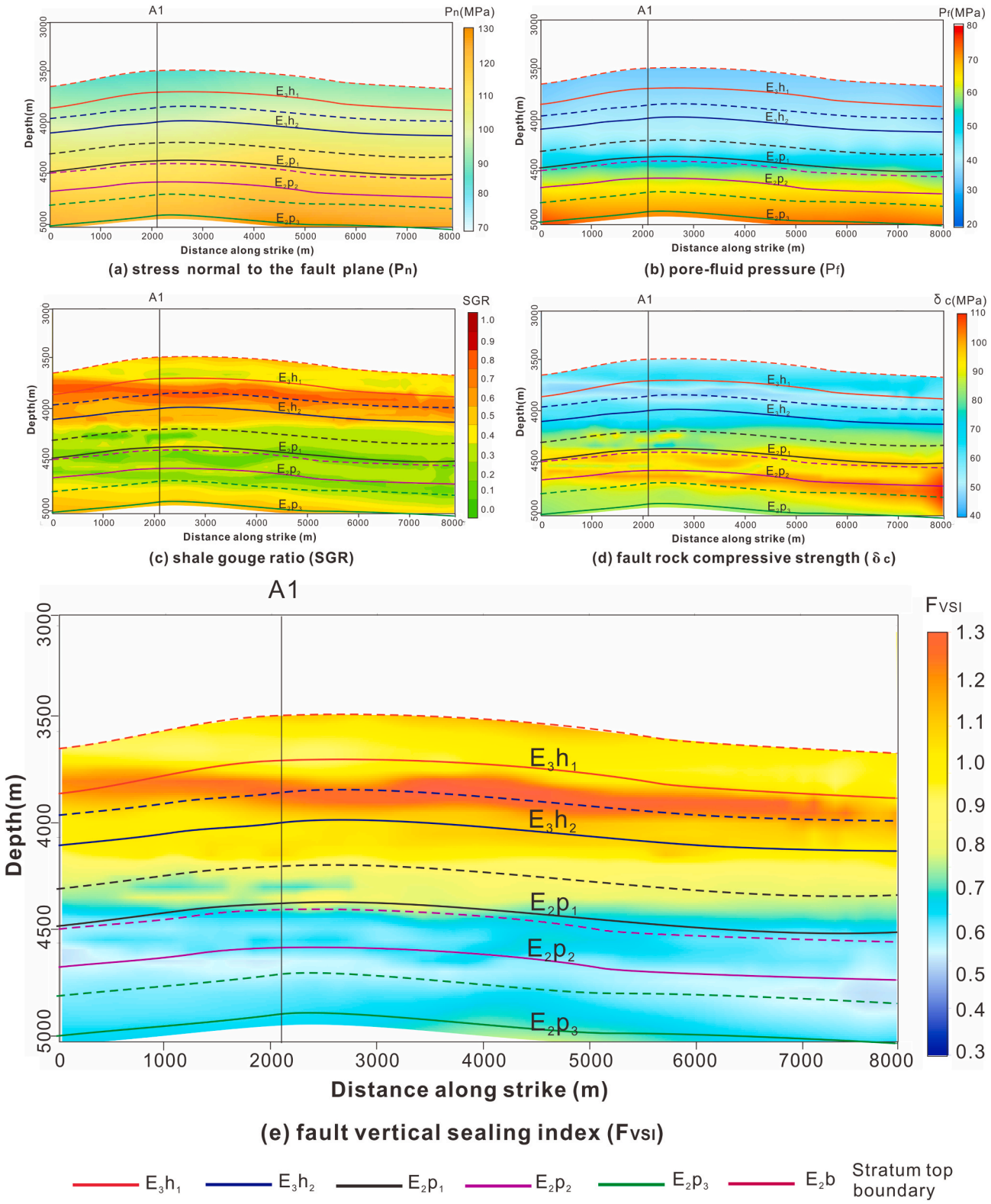

Fig. 12. (a), (b), (c), (d) and (e) are cross-sections showing the projection of the distribution of the normal stress ($\mathbf{P_n}$), pore-fluid pressure ($\mathbf{P_f}$), shale gouge ratio (SGR), fault rock compressive strength ($\boldsymbol{\delta_c}$) and fault vertical sealing index ($\mathbf{F_{VSI}}$) on the surface of the F1 fault, respectively. The solid line represents the top stratum boundary of the hanging wall, and the dashed line represents the top stratum boundary of the footwall.

(Figs. 17 and 18). Meanwhile, only a small scale of hydrocarbons characterized by a gas-water layer have accumulated in areas with a relatively low F_{VSI}(<0.5), the gas-water layer present in Wells C2 and the E_2p_3 of the Well B1 support this interpretation (Fig. 18). Thus, the fault zone may not continue to accumulate hydrocarbons when the F_{VSI} value is less than a lower limit value. According to the variation between hydrocarbons shows and the corresponding F_{VSI} value with burial depth (Fig. 19a), an F_{VSI} value of 0.4 can be confirmed as the lower limit of hydrocarbon accumulation. Therefore, in this study area, a fault zone with an F_{VSI} value less than 0.4 behaves as a conduit for vertical

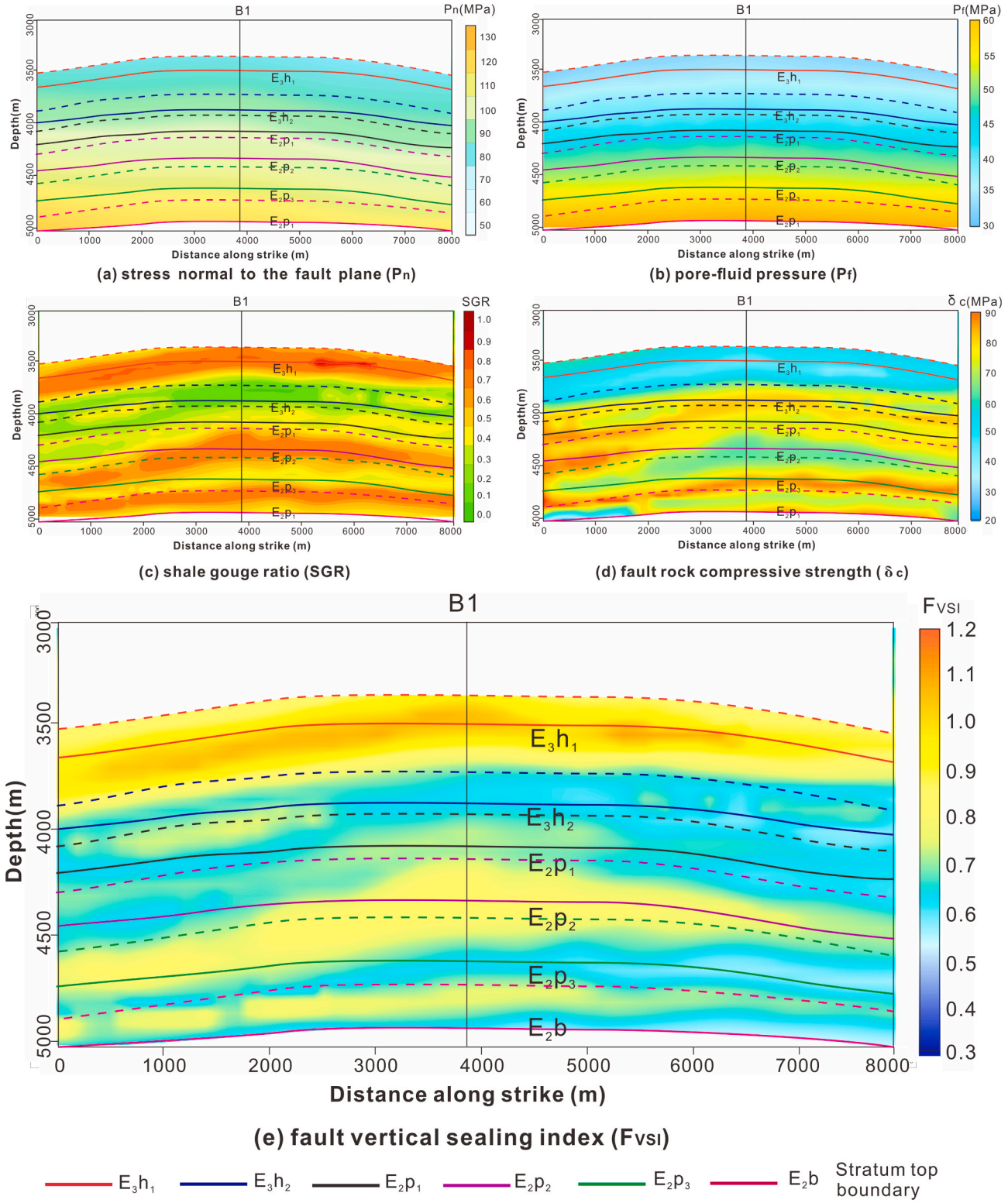

Fig. 13. (a), (b), (c), (d) and (e) are cross-sections showing the projection of the distribution of the normal stress ($\mathbf{P_n}$), pore-fluid pressure ($\mathbf{P_f}$), shale gouge ratio (SGR), fault rock compressive strength ($\boldsymbol{\delta_c}$) and fault vertical sealing index ($\mathbf{F_{VSI}}$) on the surface of the F2 fault, respectively. The solid line represents the top stratum boundary of the hanging wall, and the dashed line represents the top stratum boundary of the footwall.

migration and cannot cause hydrocarbon accumulation.

In another situation, the fault zone can seal a certain amount of hydrocarbons while continuing to transport hydrocarbons vertically, which depends on the upper limit of the hydrocarbon column height (H_{HC}) that the F_{VSI} can seal. According to the above analysis, a fault zone with an F_{VSI} value greater than 0.4 could seal a certain amount of hydrocarbons. However, when the height of hydrocarbon accumulation exceeds the upper limit that the corresponding F_{VSI} can seal, hydrocarbons continue to migrate upward. The height of the hydrocarbon column can be obtained through oil and gas testing and logging

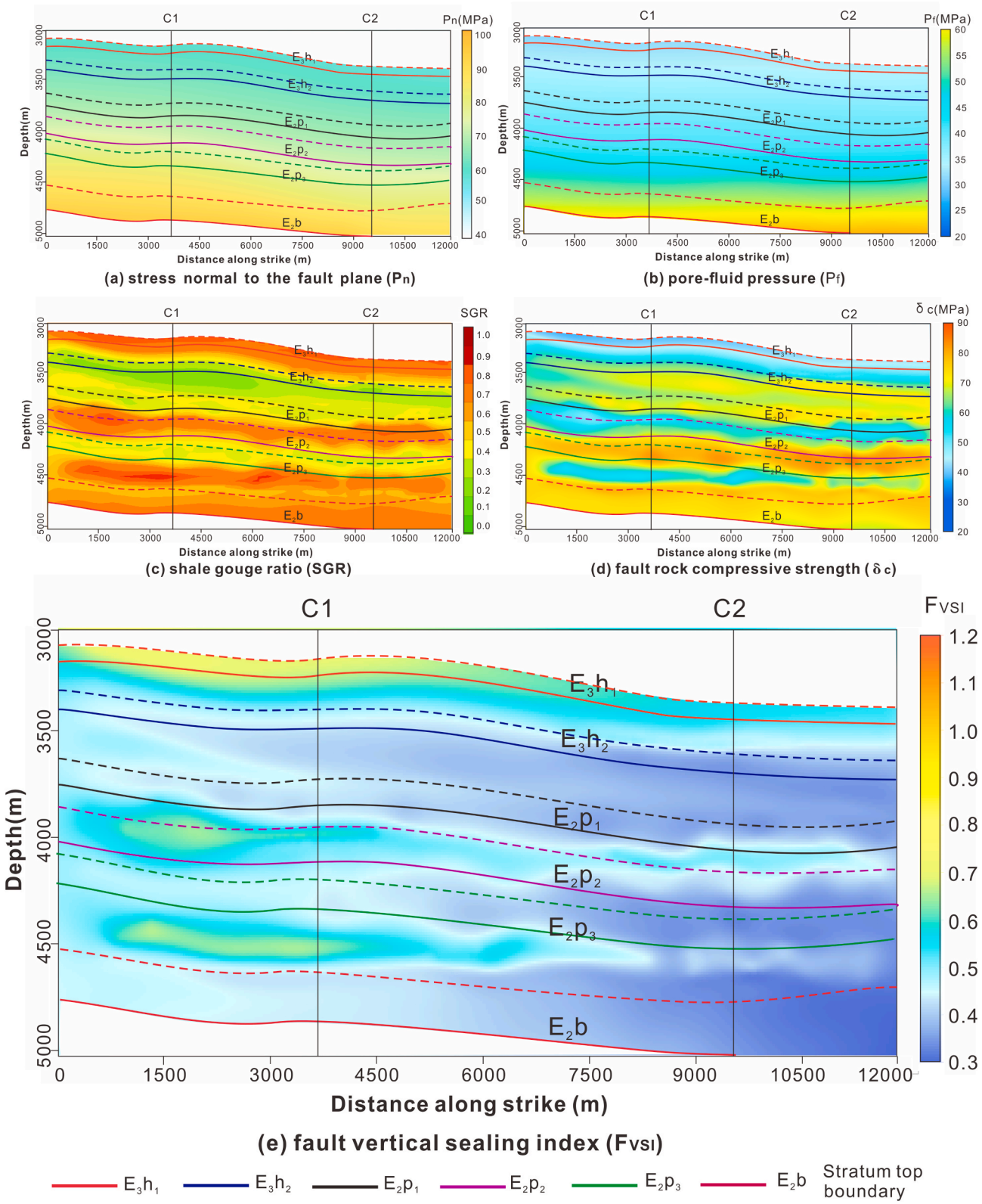

Fig. 14. (a), (b), (c), (d) and (e) are cross-sections showing the projection of the distribution of the normal stress ($\mathbf{P_n}$), pore-fluid pressure ($\mathbf{P_f}$), shale gouge ratio (SGR), fault rock compressive strength ($\boldsymbol{\delta_c}$) and fault vertical sealing index ($\mathbf{F_{VSI}}$) on the surface of the F3 fault, respectively. The solid line represents the top stratum boundary of the hanging wall, and the dashed line represents the top stratum boundary of the footwall.

interpretation data. As shown in Fig. 19b, the maximum hydrocarbon column height (H_{MHC}) that the fault rock can vertically seal is positively related to the F_{VSI} value, and the quantitative relation can be expressed as equation (11). When the F_{VSI} is less than 0.4, the height of the hydrocarbon column that the fault rock can seal vertically is 0. Equation (11) is expressed as follows:

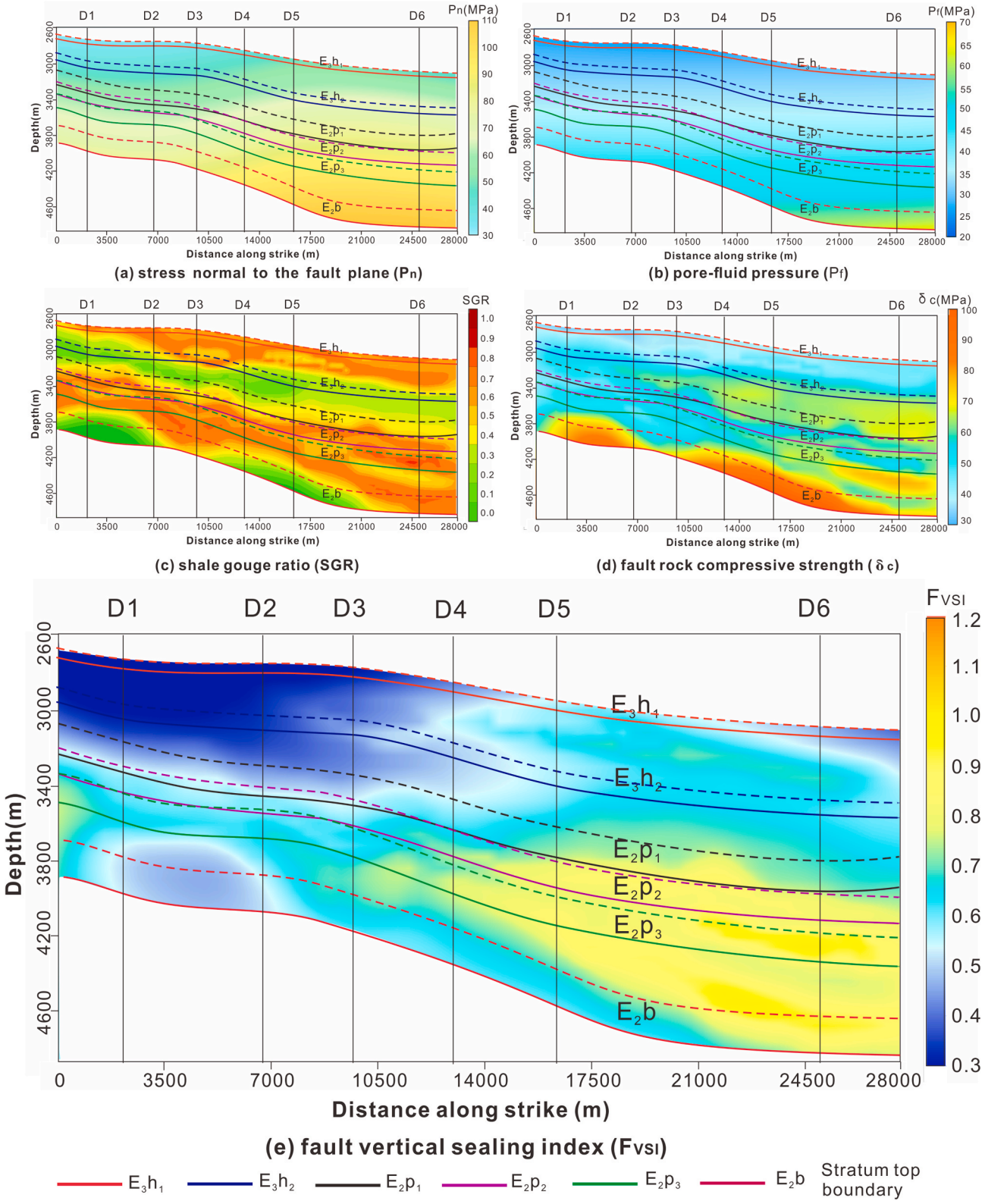

Fig. 15. (a), (b), (c), (d) and (e) are cross-sections showing the projection of the distribution of the normal stress ($\mathbf{P_n}$), pore-fluid pressure ($\mathbf{P_f}$), shale gouge ratio (SGR), fault rock compressive strength ($\boldsymbol{\delta_c}$) and fault vertical sealing index ($\mathbf{F_{VSI}}$) on the surface of the F4 fault, respectively. The solid line represents the top stratum boundary of the hanging wall, and the dashed line represents the top stratum boundary of the footwall.

$$H_{MHC} = \begin{cases} 0 & , F_{VSI} < 0.4 \\ 83.33F_{VSI} - 33.33, & F_{VSI} \geq 0.4 \end{cases} \quad (11)$$

For the F1 and F2 faults with abundant hydrocarbon sources, it is usually easier for hydrocarbons to break through the fault vertical seal and continue to migrate upward, and the vertical multilayer hydrocarbon distribution shown in Wells A1, A2 and B1 supports this interpretation (Figs. 17 and 18). However, for the F3 and F4 faults with

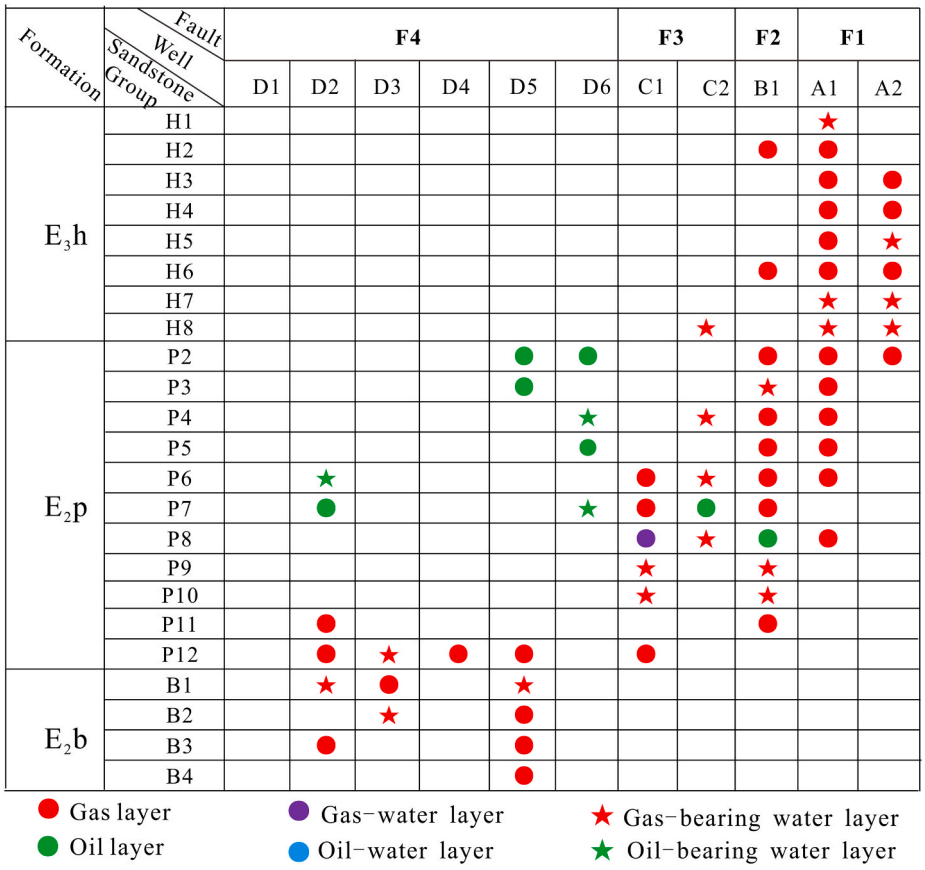

Fig. 16. Vertical hydrocarbon distribution characteristics around the F1, F2, F3, and F4 faults.

insufficient hydrocarbon sources, hydrocarbons usually accumulate in the lower position with high F_{VSI} values and cannot migrate upward. This is because hydrocarbon accumulation has difficulty reaching the H_{MHC} that the fault zone can seal. Using F4 as an example, the hydrocarbon accumulation in Well D4 was sealed below 4000 m because the H_{HC} was significantly lower than the H_{MHC} of the corresponding fault zone (Fig. 18). In detail, the H_{HC} of the shallowest hydrocarbon accumulation in Well D4 was 13.8 m, which failed to exceed the H_{MHC} of 20.8 m that can be sealed by the fault zone with an F_{VSI} value of 0.65, and resulting in the termination of vertical hydrocarbon migration. Therefore, the vertical hydrocarbon migration and accumulation process depends on the balance of the F_{VSI} of the fault rock and the height of the hydrocarbon column.

For a specific study area, when the F_{VSI} is larger than a certain value, the fault zone completely acts as a vertical barrier and cannot transport hydrocarbons. In most cases, the sandstone layers are not completely filled with hydrocarbons, and their thicknesses are less than the thickest single sandstone layer (Fig. 20). Therefore, assuming that the thickest single sandstone body is filled with hydrocarbons, the corresponding F_{VSI} value can be approximately defined as the upper limit for vertical hydrocarbon migration in the study area. According to the thickness statistics (Fig. 20), the thickest single sandstone layer in this study area is 50 m. Thus, an F_{VSI} value of 1 can be regarded as the upper limit of vertical migration of hydrocarbons in the study area (Fig. 19b). Using Well A1 near the F1 fault as an example, the vertical distribution of natural gas below 3889.1 m, where the F_{VSI} value is equal to 1, supports this interpretation (Fig. 18). Additionally, the lack of hydrocarbons in faults with F_{VSI} values greater than 1 supports this interpretation (Fig. 19a).

Therefore, the variation in the F_{VSI} can be used to analyze the migration and accumulation processes of hydrocarbons. In this study area, a fault zone with an F_{VSI} less than 0.4 completely acts as a vertical conduit and cannot seal hydrocarbons. When the F_{VSI} value is between 0.4 and 1, the fault zone has the capability to seal hydrocarbons. However, whether hydrocarbons can continue to migrate vertically depends on the upper limit of the hydrocarbon column height that the F_{VSI} can seal. A fault zone with an F_{VSI} greater than 1 completely acts as a vertical barrier and cannot transport hydrocarbons. For other areas with similar geological conditions as the EPSB or with a low exploration degree, the lower limit of vertical sealing (F_{VSI} = 0.4) and the relation between the F_{VSI} and the height of the hydrocarbon column in this article can serve as an effective reference. However, the upper limit of the F_{VSI} for the vertical migration of hydrocarbons needs to be estimated based on the specific maximum sandstone thickness.

5.2. Hydrocarbon migration and accumulation model controlled by the F_{VSI}

Due to the late hydrocarbon charging and no tectonic movement thereafter, vertical sealing of current faults can be used to effectively reflect the overall sealing characteristics of the faults during the charging period. The previous analysis of the F_{VSI} and its corresponding hydrocarbon occurrences indicated the controlling effects of fault vertical sealing on hydrocarbon migration and accumulation. According to the F_{VSI} characteristics and charging conditions of major faults, the vertical hydrocarbon migration process and the resulting hydrocarbon accumulation in the eastern Pinghu Slope Belt of the Xihu Depression can be characterized as follows (Fig. 21).

For the structurally lower position adjacent to the WSS, the F1 and F2 faults have sufficient hydrocarbon sources, which come from both the deep WSS and local mature source rocks. The F1 fault exhibits a gradually increasing F_{VSI} value from the bottom of the E_2h Formation to the E_3h Formation, suggesting a gradually increasing vertical sealing capability. Although the F_{VSI} of the fault zone is mostly greater than 0.4,

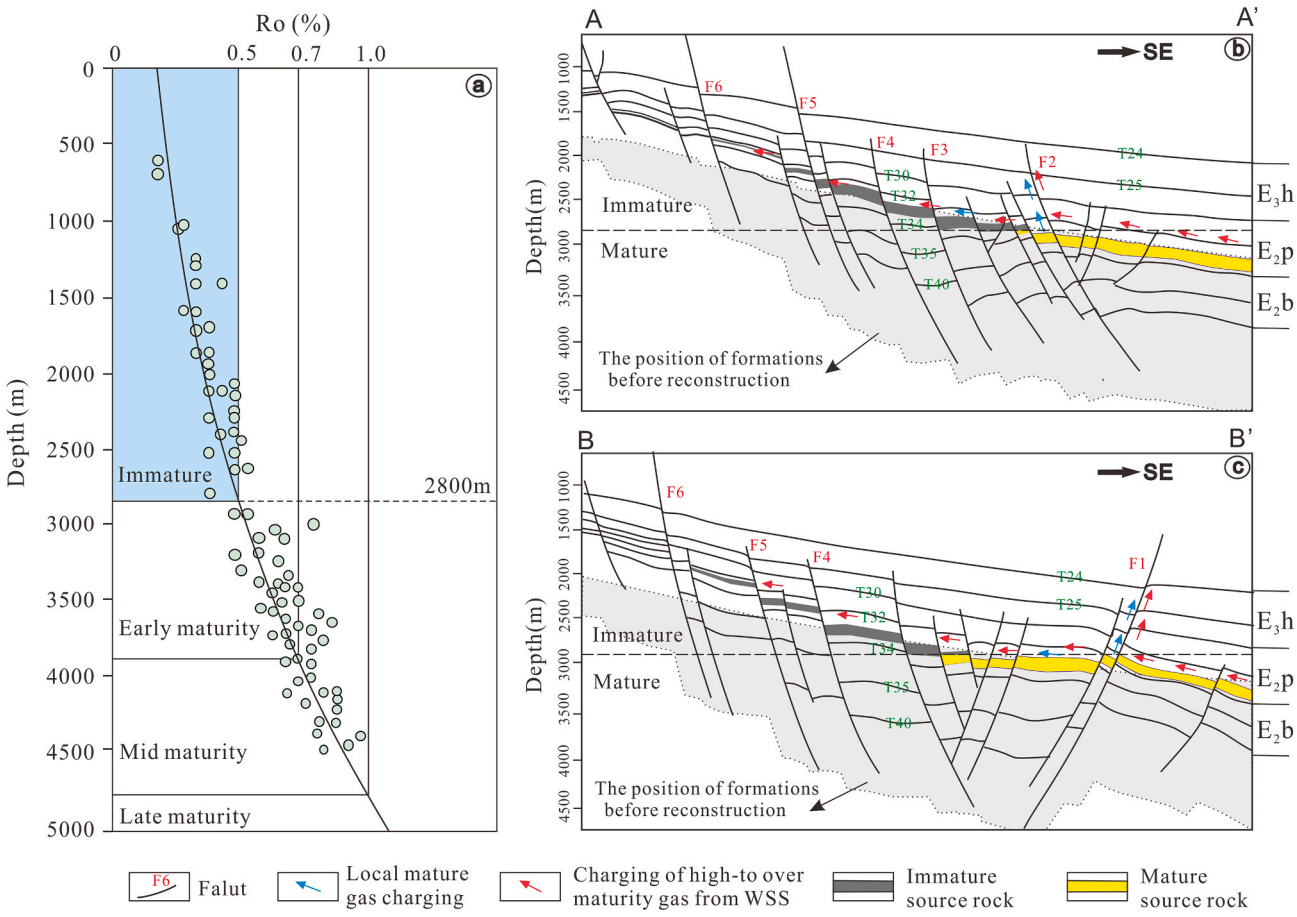

Fig. 17. (a) The variation of vitrinite reflectance (Ro) with burial depth. (b) The restored section of AA′ showing the fault distribution, source rock maturity and hydrocarbon migration direction during the main charging period. (c) The restored section of BB′ showing the fault distribution, source rock maturity and hydrocarbon migration direction during the main charging period.

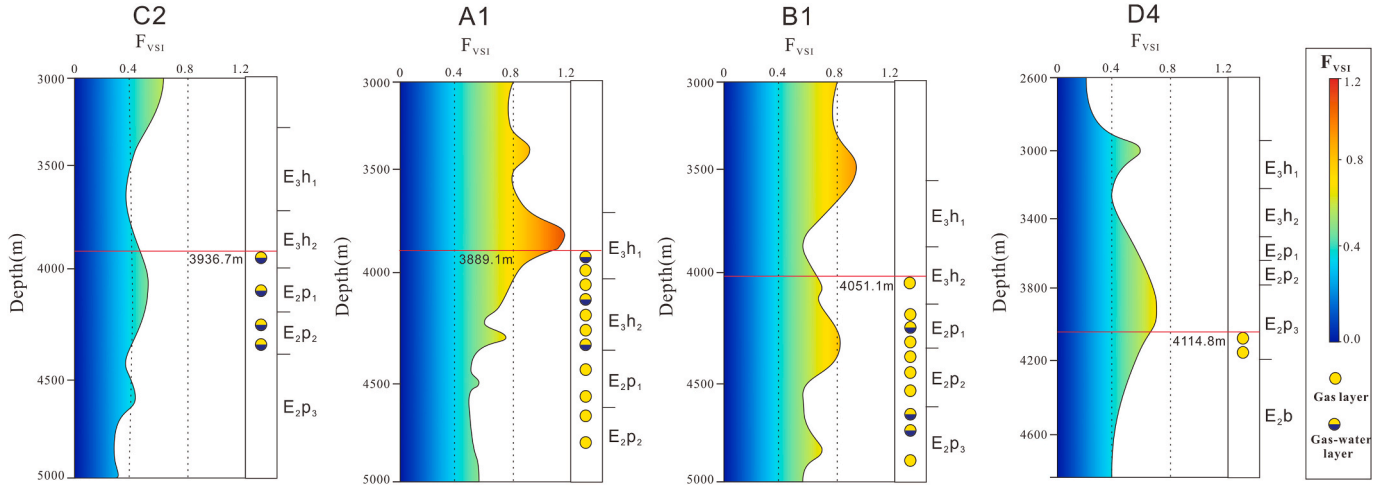

Fig. 18. The C2, A1, B1, and D4 wells show hydrocarbons and the corresponding F_{VSI} distribution in the fault zone. The red horizontal solid line marked with depth represents the shallowest burial depth where oil and gas are present. (For interpretation of the references to color in this figure legend, the reader is referred to the Web version of this article.)

sufficient charging enables hydrocarbon accumulation to break through the sealing height of the corresponding F_{VSI} and migrate vertically. Because the fault zone with an F_{VSI} greater than 1 completely acts as a barrier, the hydrocarbon accumulation near F1 is widely distributed in multiple layers below the top of the E_3h_1 member. However, the F_{VSI} distribution of the F2 fault zone corresponding to the E_2p Formation is significantly stronger than that of the F1 fault, suggesting that vertical hydrocarbon migration occurs with more difficulty. Consequently, the hydrocarbons distributed near fault F2 mainly accumulate in the E_2p Formation, except for a small amount of gas that migrates and accumulates in the relatively weakly sealed E_3h_2 member.

For structurally higher positions far away from the WSS, the hy-

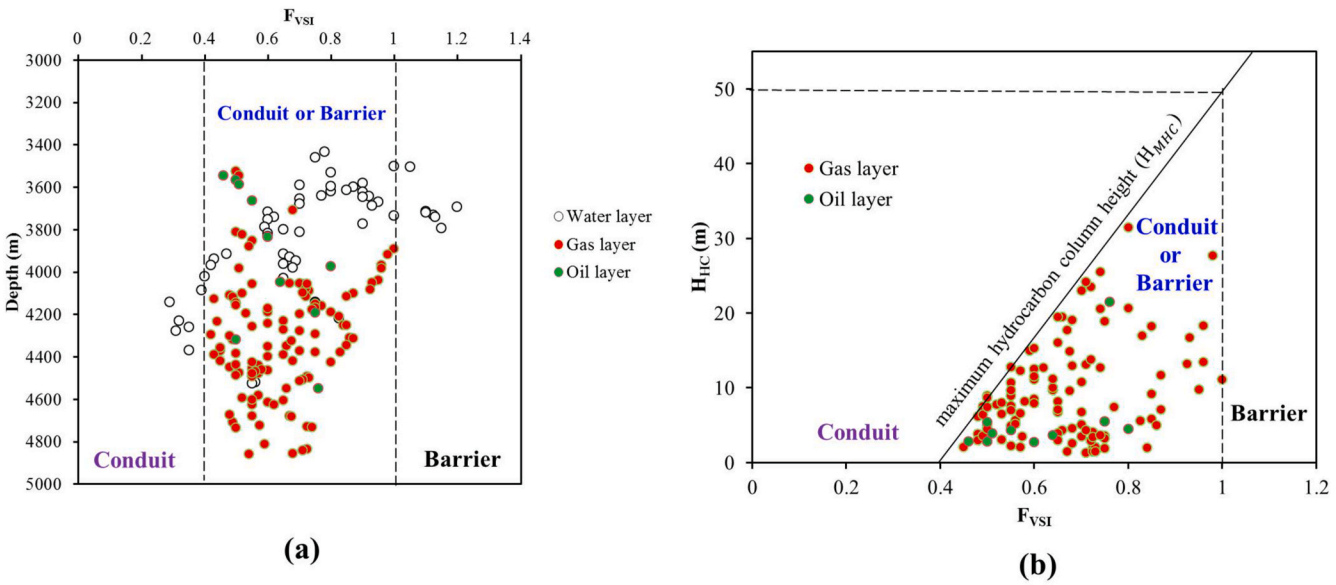

Fig. 19. (a) The relation between the fault vertical sealing index (F_{VSI}) and the corresponding oil and gas shows. (b) The variations in the fault vertical sealing index (F_{VSI}) and the corresponding hydrocarbon column height (H_{HC}).

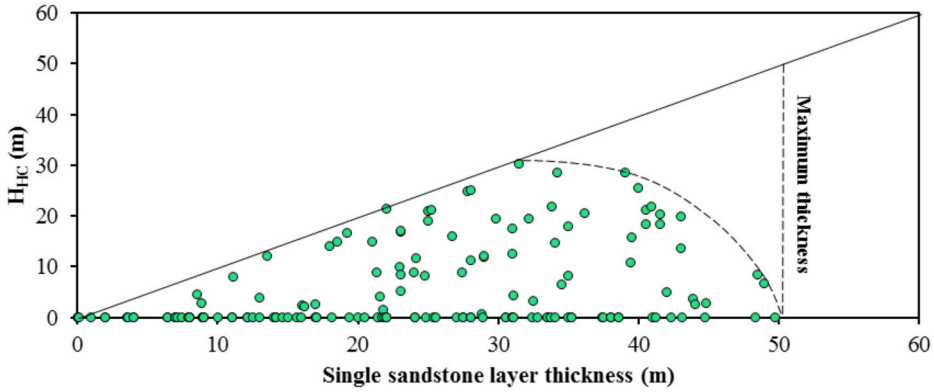

Fig. 20. The thickness of a single sandstone layer and its corresponding hydrocarbon column height (H_{HC}).

drocarbon accumulation around faults F3 and F4 mainly comes from hydrocarbons that migrated laterally along the sandstone body because the local source rock was not yet mature during the charging period. As shown in Fig. 21, the F_{VSI} distribution of the F2 and F3 fault zones corresponding to the E_2p Formation indicates relatively stronger vertical sealing. Additionally, limited hydrocarbon charging causes the accumulated hydrocarbons to be insufficient to break through the vertical seal of the fault. As a result, the hydrocarbons around F3 and F4 mainly accumulated in the E_2p Formation instead of vertically migrating into the E_3h Formation. However, the fault zone with an F_{VSI} value less than 0.4 commonly acted as a vertical conduit without hydrocarbon accumulation.

5.3. Applicability analysis

The fault vertical sealing index (F_{VSI}) method is successfully applied to reveal the relation between fault vertical sealing and hydrocarbon migration and accumulation in the EPSB of the Xihu Depression. For other petroliferous basins or regions that develop fault-bounded traps, the application of the F_{VSI} method depends on the acquisition of geological parameters, the classification of evaluation criteria and the corresponding hydrocarbon migration and accumulation analysis. The basic parameters involved in this method, such as the azimuth angle, dip angle, fault displacement, pore fluid pressure, formation density and shale content, can be easily obtained through 3D seismic data and well logging data, making evaluation operations easier for geologists. Due to the heterogeneity of fault zones and the uncertainty of geological conditions, more accurate and available data are conducive to enhancing the accuracy of the evaluation. For areas with similar geological conditions as the EPSB or with a low exploration degree, the lower limit of vertical sealing ($F_{VSI} = 0.4$) and the relation between the F_{VSI} and the height of the hydrocarbon column in this article can provide an effective reference. For areas with a relatively high degree of exploration, the evaluation criteria should be determined based on existing oil and gas shows. First, the F_{VSI} evaluation and corresponding hydrocarbon column height (H_{HC}) should be analyzed to determine the prediction model of the maximum hydrocarbon column height (H_{MHC}) that the F_{VSI} can seal. Subsequently, the corresponding F_{VSI} value when the height of the hydrocarbon column is 0 can be defined as the lower limit of the vertical sealing. In addition, the upper limit of the F_{VSI} for the vertical migration of hydrocarbons can be further estimated based on the thickest single sandstone in the study area. On the one hand, the F_{VSI} can be used to analyze whether a fault-bounded trap can capture hydrocarbons and the scale of hydrocarbon accumulation that can be sealed. Additionally, the preferential pathways of vertical hydrocarbon migration can be analyzed by the F_{VSI} to predict favorable charging positions and vertical

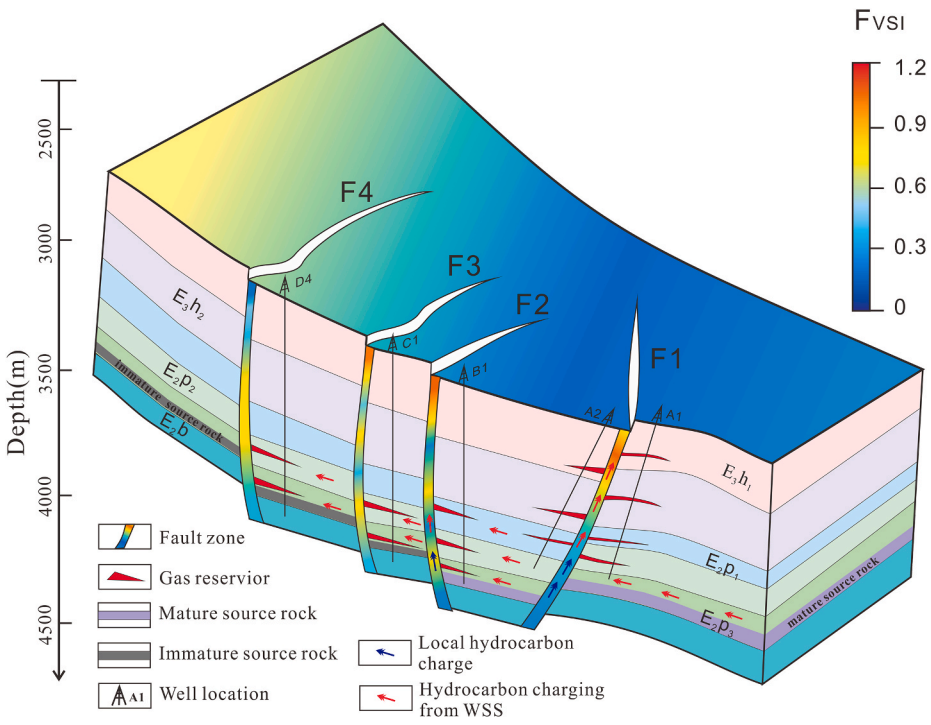

Fig. 21. Conceptual model of hydrocarbon migration and resulting accumulation in the eastern Pinghu Slope Belt of the Xihu Depression controlled by the F_{VSI}. The vertical color variation within the fault zone indicates the change in sealing capability determined by F_{VSI} (dimensionless). (For interpretation of the references to color in this figure legend, the reader is referred to the Web version of this article.)

hydrocarbon distribution ranges. Therefore, the fault vertical sealing index (F_{VSI}) method has great application potential and is also of great significance to avoid or minimize the risks of drilling and exploration. Nevertheless, this method cannot be directly applied to fault sealing evaluations in carbonate rocks. The composition of fault rock developed in carbonates is very different from those in siliciclastic rocks. Therefore, different control factors need to be considered to achieve quantitative evaluation. However, the F_{VSI} method can provide inspiration for fault analysis in carbonates.

6. Conclusions

A new parameter of the fault vertical sealing index (F_{VSI}) considering multiple factors is defined and used to quantitatively evaluate the vertical sealing of the inactive faults in the Xihu Depression. Since the vertical sealing varies with the positions on the fault surface, a fault cannot be uniformly regarded as a conduit or a barrier. Overall, fault zones with F_{VSI} values lower than 0.4 commonly act as vertical conduits. However, whether fault zones with F_{VSI} values larger than 0.4 can transport hydrocarbons vertically depends on the upper limit of the hydrocarbon column height that the F_{VSI} can seal. Meanwhile, the vertical weakly sealed fault zone is conducive to the multilayered accumulation of hydrocarbons, whereas the vertical strongly sealed fault zone results in a more concentrated hydrocarbon distribution in lower strata. Hence, the vertical sealing variation of fault controls the processes of hydrocarbon migration and accumulation and therefore the distribution of hydrocarbons.

Fault sealing has been studied for many years but this study attempts to further accurately characterize the vertical sealing variations along the faults and understand the corresponding hydrocarbon migration and accumulation process. More available data based on 3D seismic, well logging and testing analysis are needed in order to increase the validity of the interpretations from this work. The methods and conclusions involved in this article have great potential to be applied to the following analysis. (1) Integrating fault vertical sealing, geochemical tracing and migration pathways numerical simulation to reveal the vertical hydrocarbon preferential migration pathways in complex fault zones. (2) Combined with lateral hydrocarbon migration and reservoir distribution to comprehensively predict the location and scale of hydrocarbon accumulation controlled by faults, thereby reducing exploration risks in rifted basins.

Credit author statement

Fuwei Wang: Methodology, Writing – original draft, Data curation. Dongxia Chen: Conceptualization, Writing – review & editing, Supervision. Wenlei Du: Conceptualization, Visualization. Jianhui Zeng: Supervision. Qiaochu Wang: Investigation, Software. Ziye Tian: Investigation, Formal analysis. Siyuan Chang: Investigation, Software. Mengya Jiang: Investigation, Software.

Declaration of competing interest

The authors declare that they have no known competing financial interests or personal relationships that could have appeared to influence the work reported in this paper.

Acknowledgements

This work was funded by the National Natural Science Foundation of China (Grant No. 41972124). We appreciate the support from Research Institute of CNOOC Shanghai Branch and SINOPEC Shanghai Offshore Oil & Gas Company for providing data used in this study and the permission to publish the results.

References

Abbas, A., Zhu, H.T., Zeng, Z.W., Zhou, X.H., 2018. Sedimentary facies analysis using sequence stratigraphy and seismic sedimentology in the Paleogene Pinghu Formation, xihu depression, east China Sea Shelf basin. Mar. Petrol. Geol. 93, 287–297.

Allan, U.S., 1989. Model for hydrocarbon migration and entrapment within faulted structures. AAPG (Am. Assoc. Pet. Geol.) Bull. 73 (7), 803–811.
Bense, V.F., Gleeson, T., Loveless, S.E., Bour, O., Scibek, J., 2013. Fault zone hydrogeology. Earth Sci. Rev. 127, 171–192.
Bishop, A.W., 1959. The principle of effective stress. Tek. Ukebl. 106 (39), 113–143.
Blair, T.C., Bilodeau, W.L., 1988. Development of tectonic cyclothems in rift, pull-apart, and foreland basins: sedimentary response to episodic tectonism. Geology 16 (6), 517–520.
Blouet, J.P., Imbert, P., Foubert, A., 2017. Mechanisms of biogenic gas migration revealed by seep carbonate paragenesis, Panoche Hills, California. AAPG (Am. Assoc. Pet. Geol.) Bull. 101 (8), 1309–1340.
Bouvier, J.D., Kaarssijpesteijn, C.H., Kluesner, D.F., Onyejekwe, C.C., Vanderpal, R.C., 1989. Three-dimensional seismic interpretation and fault sealing investigations, Nun River Field, Nigeria. AAPG (Am. Assoc. Pet. Geol.) Bull. 73 (11), 1397–1414.
Byerlee, J.D., 1993. Model for episodic flow of high pressure water in fault zones before earthquakes. Geology 21, 303–306.
Cai, H., Zhang, J.P., 2013. Characteristics of faults on the Pinghu slope of Xihu sag, the east China Sea Shelf Basin and their sealing capability. Mar. Geol. Front. 29 (4), 20–26 (in Chinese).
Caine, J.S., Evans, J.P., Forster, C.B., 1996. Fault zone architecture and permeability structure. Geology 24 (11), 1025–1028.
Chang, C., Zoback, M.D., Khaksar, A., 2006. Empirical relations between rock strength and physical properties in sedimentary rocks. J. Petrol. Sci. Eng. 51 (3–4), 223–237.
Chen, J.R., Peng, X.M., 1994. Influence of burial depth on the properties of regional covering strata with an experimental analysis of triaxial resistance to shearing and compression. Exp. Pet. Geol. 16 (3), 282–289 (in Chinese).
Duan, M., Ye, J., Wu, J., Shan, C., Lei, C., 2017. Overpressure formation mechanism in xihu depression of the East China Sea Shelf basin. Earth Sci. 42 (1), 1935 (in Chinese).
Eichhubl, P., Boles, J.R., 2000. Rates of fluid flow in fault systems-evidence for episodic rapid fluid flow in the Miocene Monterey Formation, coastal California. Am. J. Sci. 300, 571–600.
Faulkner, D.R., Jackson, C.A.L., Lunn, R.J., Schlische, R.W., Shipton, Z.K., Wibberley, C. A.J., Withjack, M.O., 2010. A review of recent developments concerning the structure, mechanics and fluid flow properties of fault zones. J. Struct. Geol. 32, 1557–1575.
Faulkner, D.R., Lewis, A.C., Rutter, E.H., 2003. On the internal structure and mechanics of large strike-slip fault zones: field observations of the Carboneras fault in southeastern Spain. Tectonophysics 367 (3–4), 235–251.
Fisher, Q.J., Jolley, S.J., 2007. Treatment of faults in production simulation models. Geol. Soc. Lond. Spec. Publ. 292, 219–233.
Fisher, Q.J., Knipe, R.J., 1998. Fault sealing processes in siliciclastic sediments. Geol. Soc. Lond. Spec. Publ. 147 (1), 117–134.
Fisher, Q.J., Knipe, R.J., 2001. The permeability of faults within siliciclastic petroleum reservoirs of the North Sea and Norwegian Continental Shelf. Mar. Petrol. Geol. 18 (10), 1063–1081.
Fisher, Q.J., Knipe, R.J., Worden, R.H., 2009. Microstructures of deformed and non-deformed sandstones from the North Sea: implications for the origins of quartz cement in sandstones. In: Worden, R.H., Morad, S. (Eds.), Quartz Cementation in Sandstones 14. Blackwell Publishing Ltd, Oxford, UK, pp. 129–146.
Fossen, H., Schultz, R.A., Shipton, Z.K., Mair, K., 2007. Deformation bands in sandstone: a review. J. Geol. Soc. 164 (4), 755–769.
Fossen, H., Schultz, R.A., Torabi, A., 2011. Conditions and implications for compaction band formation in the Navajo Sandstone, Utah. J. Struct. Geol. 33 (10), 1477–1490.
Fu, G., Li, Y.X., Zhang, Y.F., Nie, H.J., 1997. Methods of research on fault-vertical-sealed oil & gas and its applications. Nat. Gas. Ind. 17 (6), 22–25 (In Chinese).
Fu, G., Shi, J.J., Lü, Y.F., 2012. An improvement in quantitatively studying lateral seal of faults. Acta Pet. Sin. 33 (3), 414–418 (in Chinese).
Fu, G., Wang, G.M., Huang, J.S., 2008. A method judging the experience or not of transporting oil gas ability of fault in the stillstand period. Acta Sedmentol. Sinica 26 (5), 851–856 (in Chinese).
Fu, G., Wang, P.Y., Sun, H.B., 1998. Vertical confining model of fault and its study method. Xinjing Pet. Geol. 19 (1), 7–10 (in Chinese).
Fulljames, J.R., Zijerveld, L.J.J., Franssen, R.C.M.W., 1997. Fault seal processes: systematic analysis of fault seals over geological and production time scales. In: Møller-Pedersen, P., Koestler, A.G. (Eds.), Norwegian Petroleum Society Special Publications, vol. 7, pp. 51–59.
Gartrell, A., Bailey, W.R., Brincat, M., 2006. A new model for assessing trap integrity and oil preservation risks associated with postrift fault reactivation in the Timor Sea. AAPG (Am. Assoc. Pet. Geol.) Bull. 90 (12), 1921–1944.
Gibson, R.G., 1994. Fault-zone seals in siliclastic strata of the Columbus Basin, offshore Trinidad. AAPG (Am. Assoc. Pet. Geol.) Bull. 78, 1372–1385.
Hao, F., Zhou, X., Zhu, Y., Bao, X., Yang, Y., 2009. Charging of the neogene penglai 19-3 field, bohai bay basin, China: oil accumulation in a young trap in an active fault zone. AAPG (Am. Assoc. Pet. Geol.) Bull. 93 (2), 155–179.
Hao, F., Zhu, W.L., Zou, H.Y., Li, P.P., 2015. Factors controlling petroleum accumulation and leakage in overpressured reservoirs. AAPG (Am. Assoc. Pet. Geol.) Bull. 99 (5), 831–858.
Harding, T.P., Tuminas, A.C., 1989. Structural interpretation of hydrocarbon traps sealed by basement normal blocks and at stable flank of foredeep basins and at rift basins. AAPG (Am. Assoc. Pet. Geol.) Bull. 73, 812–840.
He, P., Liu, C.W., Wang, C., You, S., Wang, W.Q., Li, L., 2011. Correlation analysis of uniaxial compressive strength and elastic modulus of sedimentary rocks. J. Sichuan Univ. (Eng. Sci. Ed.) 43 (4), 7–12 (in Chinese).
Ho, S., Carruthers, D., Imbert, P., 2016. Insights into the permeability of polygonal faults from their intersection geometries with Linear Chimneys: a case study from the Lower Congo Basin. Carnets Géol. 16 (2), 17–26.
Ho, S., Cartwright, J.A., Imbert, P., 2012. Vertical evolution of fluid venting structures in relation to gas flux, in the Neogene-Quaternary of the Lower Congo Basin, Offshore Angola. Mar. Geol. 332, 40–55.
Ho, S., Hovland, M., Blouet, J.P., Wetzel, A., Imbert, P., Carruthers, D., 2018. Formation of linear planform chimneys controlled by preferential hydrocarbon leakage and anisotropic stresses in faulted fine-grained sediments, offshore Angola. Solid Earth 9 (6), 1437–1468.
Horsrud, P., 2001. Estimating mechanical properties of shale from empirical correlations. SPE Drill. Complet. 16 (1), 68–73.
Hottman, C.E., Johnson, R.K., 1965. Estimation of formation pressures from log-derived shale properties. J. Petrol. Technol. 17 (6), 717–722.
Hubbert, M.K., Rubey, W.W., 1959. Role of fluid pressure in mechanics of overthrust faulting. Geol. Soc. Am. Bull. 70, 115–205.
Hudson, J.A., Harrison, J.P., 2000. Engineering Rock Mechanics-An Introduction to the Principles, vol. 25. Elsevier, Amsterdam, pp. 1234–1238, 8.
Indrevær, K., Stunitz, H., Bergh, S.G., 2014. On Palaeozoic–Mesozoic brittle normal faults along the SW Barents Sea margin: fault processes and implications for basement permeability and margin evolution. J. Geol. Soc. 171 (6), 831–846.
Jaeger, J.C., Cook, G., 1979. Fundamentals of Rock Mechanics. Chapman and Hall, London, p. 593.
Jolley, S.J., Barr, D., Walsh, J.J., Knipe, R.J., 2007. Structurally complex reservoirs: an introduction. Geol. Soc. Lond. Spec. Publ. 292, 1–24.
Karlsen, D.A., Skeie, J.E., 2006. Petroleum migration, faults and overpressure: calibrating basin modeling using petroleum in traps-a review. J. Petrol. Geol. 29, 227–256.
Knipe, R.J., 1993. The influence of fault zone processes and diagenesis on fluid flow. Diagenesis Basin Dev. 36, 135–154.
Knipe, R.J., 1997. Juxtaposition and seal diagrams to help analyze fault seals in hydrocarbon reservoirs. AAPG (Am. Assoc. Pet. Geol.) Bull. 81 (2), 187–195.
Knipe, R.J., Fisher, R.J., Jones, G., Clennell, M.R., Farmer, A.B., Harrison, A., Kidd, B., McAllister, E., Porter, J.R., White, E.A., 1997. Fault seal analysis: successful methodologies, application and future directions. Norwegian Petrol. Soc. Spec. Publ. 7, 15–40.
Lei, Y.H., Luo, X.R., Zhang, L.K., Cheng, M., Song, C.P., 2013. A quantitative method for characterizing transport capability of compound hydrocarbon carrier system. J. Earth Sci. 24 (3), 328–342.
Li, C.L., Kong, X.Y., Xu, X.Z., Li, P.C., 1999. Double effective stress of porous media. Nat. Mag. 21 (5), 288–292.
Li, H., Wu, J.T., Huang, J.T., Wang, Y., Li, Z.P., 2020. Quantitative analysis of fault vertical sealing ability and its application in A oilfield of Bohai Bay Basin. Bull. Geol. Sci. Technol. 39 (4), 125–131 (in Chinese).
Lindsay, N.G., Murphy, F.C., Walsh, J.J., Watterson, J., 1993. Outcrop studies of shale smears on fault surface. In: The Geological Modelling of Hydrocarbon Reservoirs and Outcrop Analogues. Blackwell Publishing Ltd, pp. 113–123.
Lü, Y.F., Huang, J.S., Fu, G., Fu, X.f., 2009. Quantitative study On fault sealing ability in sandstone and mudstone thin interbed. Acta Pet. Sin. 30 (6), 824–829 (In Chinese).
Lü, Y.F., Li, G.H., Wang, Y.W., Song, G.J., 1996. Quantitative analyses in fault sealing properties. Acta Pet. Sin. 17 (3), 39–45 (in Chinese).
Luo, X.R., 2004. Quantitative analysis on overpressuring mechanism resulted from tectonic stress. Chin. J. Geophys. 47, 484–493 (in Chinese).
Magara, L.J., 1968. Compaction and migration of fluids in Miocene mudstone, Nagaoka plain, Japan. AAPG (Am. Assoc. Pet. Geol.) Bull. 52 (12), 2466–2501.
Manzocchi, T., Childs, C., 2013. Quantification of hydrodynamic effects on capillary seal capacity. Petrol. Geosci. 19 (2), 105–121.
McNally, G.H., 1987. Estimation of coal measures rock strength using sonic and neutron logs. Geoexploration 24, 381–395.
Ottesen Ellevset, S., Knipe, R.J., Svava Olsen, T., Fisher, Q.J., Jones, G., 1998. Fault controlled communication in the Sleipner Vest Field, Norwegian Continental Shelf; detailed, quantitative input for reservoir simulation and well planning. Geol. Soc. Lond. Spec. Publ. 147 (1), 283–297.
Pei, Y.W., Paton, D.A., Knipe, R.J., Wu, K.Y., 2015. A review of fault sealing behaviour and its evaluation in siliciclastic rocks. Earth Sci. Rev. 150, 121–138.
Peng, X.M., 1993. Study on the buried depth and thickness standard of the regional caprock with the experimental method of rock mechanics. In: Shi, BaoHeng, Zhou, Kun, Guang, DeiFan (Eds.), Xu ZhiChuan. Yangtze Marine Geology and Petroleum. Petroleum Industry Press, Beijing, pp. 262–269 (in Chinese).
Schowalter, T.T., 1979. Mechanics of secondary hydrocarbon migration and entrapment. AAPG (Am. Assoc. Pet. Geol.) Bull. 63 (5), 723–760.
Schultz, R.A., Fossen, H., 2008. Terminology for structural discontinuities. AAPG (Am. Assoc. Pet. Geol.) Bull. 92 (7), 853–867.
Shan, C., Ye, J.R., Cao, Q., Lei, C., Peng, Y., Tian, Y., 2015. Controlling factors for gas accumulation in kongqueting gas field of Xihu Sag. Mar. Geol. Quat. Geol. 35 (1), 135–144 (in Chinese).
Sibson, R.H., 1990. Conditions for fault-valve behaviour. Geol. Soc. Lond. Spec. Publ. 54 (1), 15–28.
Sibson, R.H., Moore, J.M.M., Rankin, A.H., 1975. Seismic pumping - a hydrothermal fluid transport mechanism. J. Geol. Soc. 131 (6), 653–659.
Smith, D.A., 1966. Theoretical considerations of sealing and non-sealing faults. AAPG (Am. Assoc. Pet. Geol.) Bull. 50 (2), 363–374.
Smith, D.A., 1980. Sealing and nonsealing faults in Louisiana Gulf Coast salt basin. AAPG (Am. Assoc. Pet. Geol.) Bull. 64 (2), 145–172.
Song, X.Y., Chu, C.L., Rui, Z.F., 2010. Structural framework and evolution of xihu sag in east China sea basin. Geol. J. China Univ. 16 (1), 86–93 (in Chinese).

Su, A., Chen, H.H., Ma, Y.H., Zhan, H.Y., Yang, W.S., 2015. Geologic conditions and main controlling factors of gas washing in Kongqueting region in Xihu Depression, Eastern Sea Basin. Nat. Gas Geosci. 26 (2), 292–300 (in Chinese).
Su, A., Chen, H.H., Zhao, J.X., Zhang, T.W., Feng, Y.X., Wang, C.W., 2020. Natural gas washing induces condensate formation from coal measures in the Pinghu Slope Belt of the Xihu Depression, East China Sea Basin: insights from fluid inclusion, geochemistry, and rock gold-tube pyrolysis. Mar. Petrol. Geol. 118.
Sun, D.Z., Zhang, H.S., Duan, F.F., Yan, W.F., Shi, X.C., 2016. Experimental study on mechanics and drillability of lower strata rock in central subsag of Xihu sag. China Offshore Oil Gas 28 (1), 93–97 (in Chinese).
Tang, W., Zhao, X.B., Lei, J.Y., Yuan, B., Liu, H.W., 2016. Numerical simulation on the size effect of compressive strength and deformation parameters of rock materials under different confining pressures. Geol. J. China Univ. 22 (3), 580–588 (in Chinese).
Terzaghi, K., 1923. Die Berechnung der Durchassigkeitsziffer des Tones aus dem Verlauf der hydrodynamischen Spannungserscheinungen. Akademie der Wissenschaften in Wien 132 (3/4), 125–138.
Tian, H., Zha, M., Shi, X.P., Hu, P., 2003. Calculation of fault tightness index and its significance for fault sealing. Xinjing Pet. Geol. 24 (6), 530–532 (in Chinese).
Tong, H.M., 1998. Quantitative analysis of fault opening and sealing. Oil Gas Geol. 19 (3), 215–220 (in Chinese).
Wang, Y., Li, Z.M., Wang, D.X., Zhao, L., Zhang, D.Y., Wen, H.B., 2005. The establishment of regression model for rock compressive strength. Fault-Block Oil Gas Field 12 (2), 17–19 (in Chinese).
Webster, M., O'Connor, S., Pindar, B., Swarbrick, R., 2011. Overpressures in the taranaki basin: distribution, causes, and implications for exploration. AAPG (Am. Assoc. Pet. Geol.) Bull. 95 (3), 339–370.
White, N.J., Jackson, J.A., McKenzie, D.P., 1986. The relationship between the geometry of normal faults and that of the sedimentary layers in their hanging walls. J. Struct. Geol. 8 (8), 897–909.
Xu, H.Y., George, S.C., Hou, D.J., Cao, B., Chen, X.D., 2020. Petroleum sources in the Xihu Depression, East China Sea: evidence from stable carbon isotopic compositions of individual n-alkanes and isoprenoids. J. Petrol. Sci. Eng. 190, 107073.
Xu, Z.H., Wu, X., 1996. Characteristics of contemporary tectonic stress in Beidagang oil field and its vicinity. Petrol. Explor. Dev. 23 (6), 78–81 (in Chinese).
Xu, Z.H., Xu, G.Q., Wu, S.W., 1999. Discussion on the present-day tectonic stress field and its cause in the East China Sea. Acta Seismol. Sin. (Chin. Ed.) 21 (5), 495–501 (in Chinese).
Xu, Z.H., Wu, S.W., 1997. A study on present-day tectonic stress in the southern yellow sea and East China Sea region. ACTA GEOPHYSICA SINICA 40 (6), 773–781 (in Chinese).
Yang, C.H., Zeng, G.D., Li, S.Q., Liang, R.B., 2014. Fault development characteristics and hydrocarbon accumulation in Pingbei area of xihu sag, east China sea. Petrol. Geol. Exp. 36 (1), 68–69+82 (in Chinese).
Ye, J., Qing, H., Bend, S.L., Gu, H., 2007. Petroleum systems in the offshore xihu basin on the continental shelf of the east China sea. AAPG (Am. Assoc. Pet. Geol.) Bull. 91 (8), 1167–1188.
Yielding, G., Freeman, B., Needham, D.T., 1997. Quantitative fault seal prediction. AAPG (Am. Assoc. Pet. Geol.) Bull. 81 (6), 897–917.
Zhang, J., Lu, Y., Krijgsman, W., Liu, J.H., Li, X.Q., Du, X.B., Wang, C., Liu, X.C., Feng, L., Wei, W., Lin, H., 2018. Source to sink transport in the Oligocene Huagang formation of the xihu depression, east China Sea Shelf basin. Mar. Petrol. Geol. 98, 733–745.
Zhang, J.P., 2013. fault system and its genetic mechanism in the Pinghu slope of the xihu sag in the east China Sea Shelf basin. Chin. J. Geol. 48 (1), 291–303 (in Chinese).
Zhang, L.K., Luo, X.R., Liao, Q.J., Yang, W., Vasseuret, G., Yu, C.h., Su, J.q., Yuan, S.Q., Xiao, D.Q., Wang, Z.M., 2010. Quantitative evaluation of synsedimentary fault opening and sealing properties using hydrocarbon connection probability assessment. AAPG (Am. Assoc. Pet. Geol.) Bull. 94 (9), 1379–1399.
Zhang, M.L., Tan, C.X., Wang, Z., 2002. A study on tectonic stress field numerical simulation and its application in Xihu Sag of East China Sea Basin. J. Geomechanics 8 (3), 229–238 (in Chinese).
Zhang, Y., Gartrell, A., Underschultz, J.R., Dewhurst, D.N., 2009a. Numerical modelling of strain localization and fluid flow during extensional fault reactivation: implications for hydrocarbon preservation. J. Struct. Geol. 31 (3), 315–327.
Zhang, Y.X., Ye, J.R., Su, K.L., Li, L.X., Xu, J.J., 2009b. The burial history and evolution of Xihu Depression. Geotect. Metallogenia 33 (2), 215–223 (in Chinese).